ANALYTICAL TECHNIQUES TO OPTIMIZE TRACE INSECTICIDE DETECTION MECHANISMS USING SURFACE PLASMON RESONANCE AND SURFACE-ENHANCED RAMAN SPECTROSCOPY

A Thesis

Presented to the Faculty of the Graduate School

of Cornell University

in Partial Fulfillment of the Requirements for the Degree of

Master of Science

By

Adrienne L. Phifer

May 2013

ABSTRACT

This thesis uses Surface Plasmon Resonance (SPR) and Surface-Enhanced Raman Spectroscopy (SERS) to optimize trace insecticide detection mechanisms. Traditional methods for trace insecticide detection include Gas Chromatography (GC)/Mass Spectrometry (MS) and Enzyme Linked Immunosorbent Assay (ELISA) methods. Although standard, these methods require large sample volumes and extensive sample preparation. A diagnostic method overcoming these issues is SERS. SERS increases the Raman signal of an analyte by chemisorption of the molecule to the surface of a noble metal or excitation of surface plasmon resonance at the metal surface. To optimize SERS enhancement factors we have used aptamers to increase a molecule's SERS signal by bringing the molecule in closer proximity to the metal surface. In this thesis, the efficiency of two malathion-specific aptamers is quantified using surface plasmon resonance techniques. Additionally, a novel Surface-Enhanced Raman Diagnostic Membrane is utilized for insecticide residue analysis.

BIOGRAPHICAL SKETCH

Adrienne L. Phifer was born in Atlanta, GA on February 21st 1989 to Carolyn Phifer and Edwin Phifer. She grew up in Decatur, GA where she attended Chapel Hill Elementary School, Narvie J. Harris Elementary Theme School, and Chapel Hill Middle School. She graduated from Southwest DeKalb High School in 2007 with honors.

She attended the University of Georgia from 2007 to 2011 where she received a Bachelor of Science in Food Science and Technology. While at the University of Georgia, she received a Peach State Louis Stokes Alliance for Minority Participation GPA Award/ Outstanding Participation Award, a John Ayers Scholarship, a E.G. Dawson Scholarship, and a Rita Waters Scholarship for academic performance and community involvement. In the fall of 2011, Adrienne began the Master of Science program in the Field of Food Science and Technology with a minor in Food Microbiology and a concentration in Plant Pathology at Cornell University. While in the Dr. Carl A. Batt laboratory at Cornell University, she mastered various analytical techniques such as Surface Plasmon Resonance, Scanning Electron Microscopy, and Surface-Enhanced Raman Spectroscopy.

To my family, whose unconditional support encourages me in all my endeavors.

ACKNOWLEDGMENTS

I would like to graciously acknowledge my advisor Dr. Carl A. Batt for his guidance and encouragement during my journey at Cornell University. His high expectations for my research inspired me to push myself harder than I ever have before. Before coming to Cornell University, no one has challenged me as much to step outside of my academic comfort zone. I am truly honored to have had the opportunity to work with such a respected person as Dr. Batt. I would also like to acknowledge my minor advisor Dr. Wayne Wilcox for being a committed and helpful member of my committee. Also, I would like to thank Dr. Wilcox for helping me learn more about a major aspect of my research.

Further, I would like to acknowledge Dr. Cameron Bardliving, Dr. Francisco Barahona Ruiz, and Stephanie Parker for all of their assistance and encouragement with my research endeavors. I would also like to thank them for being great friends, giving me brotherly and sisterly advice, and making the lab an enjoyable and comfortable place to work. I would also like to acknowledge Dr. Aaron Strickland and Mike Canfield for all of their assistance with data acquisition and analysis.

I would also like to acknowledge my family and friends for their constant support and encouragement during my academic career. I would like to thank my parents for teaching me about the importance of succeeding in academia and for guiding me to become the person I am today. I would like to thank my brother and sister for their constant support in all aspects of my life.

TABLE OF CONTENTS

Chapter 1: Introduction

SPECTROSCOPY TECHNIQUES

Spectroscopic Techniques

Spectroscopy is an analytical technique that quantifies the interaction of energy with matter. Spectroscopic techniques can range from Vibrational Spectroscopy, such as Raman Spectroscopy and Surface-Enhanced Raman Spectroscopy (SERS), UV-Vis Spectroscopy, Mass Spectroscopy, Surface Plasmon Resonance spectroscopy (SPR), and Nuclear Magnetic Resonance spectroscopy (NMR)[2-6]. These spectroscopic techniques are used to quantify matter or examine a physical process in relation to matter. This thesis will focus on the techniques of Raman Spectroscopy, Surface- Enhanced Raman Spectroscopy, and Surface Plasmon Resonance.

Raman and Surface Enhanced Raman Spectroscopy

Raman spectroscopy is a vibrational spectroscopy technique that analyzes the inelastic scattering of incident photons defined as the energy required to excite a reemitted photon to a different vibrational or rotational state[7]. The scattering corresponds to a characteristic band that parallels a specific molecular structure. The characteristic bands result in a fingerprint specific to the analyte of interest[8]. Raman spectroscopy has been praised for its specificity, easy sample preparation, and ability to be used with dry or liquid samples.

The Raman phenomenon was first observed in the late 1920s as C.V. Raman investigated the inelastic molecular scattering of light in a liquid phase along with Krishnan[2, 8-10]. Their investigations were preceded by Smekal's prediction of inelastic light scattering in the early 1920s[9]. Inelastic light scattering was also observed in crystals in the late 1920s by Landsberg and

Mandelstam[11]. Despite these discoveries, however, the Raman effect was still limited due to the inherent weakness of inelastic scattering. This limitation was improved with the development of the laser in the 1960s[2].

Since the 1960s, Raman spectroscopy has advanced even further with the development of SERS[7]. SERS techniques date back to the 1970s with the analysis of pyridine using Ag electrodes by Fleischmann *et al* [12-15]. Jeanmaire and Van Duyne concluded that the Raman amplification of pyridine near the surface of the Ag electrodes was due to its proximity to the noble metal surface[12, 14]. This amplification in Raman signal was attributed to two mechanisms: an electromagnetic enhancement (EM) and chemical enhancement[12, 14]. The EM enhancement is responsible for a greater proportion of the total signal amplification, ranging from 10^6 to 10^{11}. The EM effect results from the enhancement of surface plasmon resonance at the metal surface[2]. A plasmon is the total excitation experienced by electron gas at the surface of the metal. These surface plasmons can be localized at the metal surface or propagate along the surface of the metal[16]. The EM enhancement depends on the structure of the substrate, the surface chemistry of the substrate, and the distance of the molecule from the substrate surface[17]. Molecules further from the surface of the substrate have less of a signal enhancement[17]. Ideal distance between the molecule and the substrate surface should be in the nanometer range. The chemical enhancement is observed when the analyte's electrons interact with the electrons from the noble metal resulting in a charge transfer[2, 16, 17]. The degree of charge transfer varies between molecules[18]. The chemical enhancement contributes approximately 10^2 of the total SERS signal enhancement and is not dependent upon the EM [2, 16, 17].

Types of SERS particles

The production of reproducible, inexpensive substrates is an aspect of SERS that has gained much attention. The ability to observe large, consistent enhancement factors is vital to the success of the technique[2]. The magnitude of the enhancement factor is often influenced by the presence of hotspots, which are defined as the space between closely assembled nanoparticles that result in amplified signal enhancements[19]. Thus, in aims of optimizing the presence of SERS hotspots, many researchers point towards the use of Au or Ag nanoparticles arranged on a supporting substrate[2, 18]. Freeman *et al* for example assembled Au and Ag nanoparticles onto polymer coated substrates to increase the presence of SERS hotspots[18, 20]. Freeman *et al* took advantage of the interaction of thiol, amine, and cyanide functional groups with the Au and Ag surfaces to form monolayers. The monolayers resulted in reproducible enhancements on the nanometer scale with low variability between substrates[18, 20]. The low variability between substrates was illustrated as Freeman *et al* exhibited less than a 10% deviation between eight SiO_2 substrates functionalized with Ag nanoparticles[18]. Maxwell *et al* also fabricated AgNP monolayers in the form of a film to optimize the presence of SERS hotspots[18, 21]. The film was a polycarbonate membrane that supported the AgNPs with diameters of 100 nm and above[18]. The films were concluded to be efficiently reproducible tools for SERS detection of biological molecules[21].

As researchers began to optimize the reproducibility of SERS substrates, the tuneability of substrates became another important factor. Many researchers began to observe the effects of slight changes in nanoparticle dimensions on SERS signals. One method to analyze these effects is to fabricate substrates in the forms of nanospheres, nanogaps, and nanoshells and vary the

diameter of the nanoparticle[22-25]. Chen and Liu for example fabricated AgNP nanospheres with a silver/carbon core for the detection of melamine. The nanospheres were able to detect melamine with a detection limit of 5.0×10^{-8}M. An inverse relationship was concluded to exist between the SERS signal and the concentration of the Ag ions. The concentration of the Ag ions was inversely related to their diameters[26].

Lee *et al* also analyzed this phenomenon by fabricating nano-dumbbells consisting of a Au core, Ag shell, and nanogaps ranging from 4.8nm to <1nm[27]. Lee *et al* compared the effects of particle size and inter-particle distance on SERS intensity and enhancement factors. The particles varied from a 23-30nm pair to a 50-60nm pair. The nano-dumbbells with nanogaps <1nm resulted in enhancement factors with the least variation. Particles >50nm were found to have stronger SERS signals[27]. In addition, Zhang *et al* illustrated the importance of tunable substrates through their fabrication of Pd shells polymerized onto Au nanorod cores[28]. The Pd/Au complexes exhibited strong longitudinal surface plasmon resonance that was dependent on the thickness of the Pd shell. The SERS signals could be attributed to the Au nanorod core when the Pd shell had a thickness <2.5nm. Further, the SERS signal could be improved by tuning the aspect ratio of the Au core to the Pd shell[28].

With the advancement of tunable substrates, researchers can also enhance a molecule's Raman signal further by taking advantage of self-assembled monolayers (SAM)[29-33]. SAMs assist in bringing molecules closer to the substrate's surface and thus increase the molecule's signal further[19]. Being able to modify the surface of these noble metals with various entities such as

analyte-specific oligonucleotides has resulted in the ability of SERS to detect single molecules within a complex matrix[34].

Such an increase in SERS signal from a SAM was illustrated by Mosier-Boss[35]. Mosier-Boss immobilized AgNPs and AuNPs onto magnetic microparticles with active amine groups. The AgNPs and AuNPs were then reacted with thiols to form a SAM. The SAM was concluded to increase the SERS signal of naphthalene with constant laser exposure. This increase in SERS signal was attributed to the EM enhancement effect afforded by the SAM[35]. DeVault and Sepaniak showed similar results with their SAM formed by deposition of AgNPs, with diameters of 100nm, onto frosted glass slides[36]. After SERS spectra of benzyloxyresorufin, resorufln, and riboflavin were obtained using the AgNP SAM, DeVault and Sepaniak concluded that the sensitivity of the SERS signal increased due to the SAM.

SERS Applications

In addition to the availability of reproducible and tunable substrates functionalized with SAMs, SERS is also desired for its ability to conduct real-time analysis of trace analytes, lack of expensive reagents, and ability to process water samples with minimal background noise[2]. SERS is applicable in several entities such as environmental monitoring, pharmaceutical detection, and homeland security[2, 37-39].

SERS has been used for the detection of trace environmental analytes such as fungicides for example. Carbendazim is a benzimidazole fungicide widely used to minimize a broad spectrum of plant diseases. The SERS detection of carbendazim in the 50 μM range was achieved using

cyclodextrin inclusion complexes on gold nanorods[39]. A detection limit of 50 µM for carbendazim using the receptor1-gold nanorod complex was observed and resulted in the conclusion that receptor 1 has a significant influence on the intensity of carbendazim SERS signal[39].

SERS has also been used to detect an important insecticide with environmental and food safety implications, malathion. Malathion is a widely used aliphatic organophosphate insecticide effective against a broad spectrum of pests. An aptasensor was created based on polymer-gold nanoparticles composite microspheres for detection of malathion using SERS[40]. The aptasensor was comprised of polymer microspheres, consisting of EGDMA, MAA, and AIBN, functionalized with gold nanoparticles and malathion-selective aptamers. As a variation, AuNPs were also allocated onto glass coverslips in a microwell dish and functionalized with aptamers targeted for malathion[40].

SERS spectra obtained from the glass-AuNPs-aptamer sensors incubated with various concentrations of malathion (thiol-C_6-M17-F) revealed a positive correlation between the concentration of immobilized DNA and signal intensity. SERS spectra obtained from the polymer-AuNP-aptamer complexes incubated with a concentration of malathion illustrated several matching wave numbers characteristic for malathion. Further, these wave numbers were not present in SERS spectra prior to aptamer functionalization of the polymer-AuNPs complex[40]. Thus, the creation of this polymer-AuNP-aptamer complex has the ability to detect malathion and enhance its raman signal.

In relation to pharmaceutical applications, Mecker *et al* used SERS to detect the presence of melamine in adulterated products[41]. Melamine is a nitrogen-rich base that has been involved in several food industry controversies because its addition to milk, infant formula, and pet food as a source of nitrogen results in a misleading analysis of the product's protein content[42]. Melamine has been found to have adverse effects on human health including kidney disease and thus the ability to detect melamine in trace concentrations is important[42]. Mecker *et al* synthesized AuNPs covered with citrate and agglomerated with IPA to increase the SERS signal of melamine by 10^5. Mecker *et al* achieved a detection limit of 100-200 mu g L^{-1}. With conclusion of their efforts, Mecker *et al* created the first portable means of detecting melamine using AuNPs and SERS techniques[41]. In relation to homeland security applications, Ryu *et al* used SERS to detect an Anthrax biomarker in the form of a protective antigen[43]. AuNPs functionalized with a short 16-amino acid peptide and a Raman reporter were used to detect the protective antigen down to 6.1 fM. With conclusion of the investigation, the AuNP-peptide-reporter complex was deemed an efficient means to detect the biological hazard indicator[43].

Surface Plasmon Resonance (SPR)

SPR is spectroscopic technique based on analysis of wave optics. SPR is advantageous because of its ability to analyze sensitive changes in refractive index and layer thickness[44]. Within the flow cell of a SPR system, a specific electron density occurs between the running buffer and the surface of the SPR chip. The electron density forms plasmons at the metal surface that results in a particle when joined with a photon of incident light. This particle runs along the surface of the metal until it is absorbed. The resulting change in refractive index is measured by the change in total incident light absorbed on the metal surface[45]. Thus, when a binding phenomenon occurs at

the surface of the chip, change in refractive index between the two surfaces is quantified in Refractive Index Units (RIU)[46]. The magnitude of the change in refractive index is influenced by the size of the analyte and the conformational change the ligand experiences upon analyte binding[45].

SPR immunoassays date back to the early 1980s as Liedberg analyzed the shift in refractive index observed as antihuman γ-globulin (a-IgG) formed a s monolayer on immobilized human γ-globulin (IgG)[47]. The IgG antibody formed a monolayer 50 Å thick on a Ag film resulting in a sufficient material to detect a-IgG using SPR. The antibody-antigen relationship of the IgG and a-IgG was irreversible, however, and needed to be refreshed between analyses. Despite the irreversible nature of the system, the use of the IgG antibody was advantageous because of its reproducibility and ability to be fabricated in large quantities[47]. With conclusion of these early experiments, Liedberg forecasted the development or SPR techniques with reversible monolayer applications[47]. Such reversible applications were later exhibited as researchers immobilized ligands such as GST, pterin cofactors, and oligohistidine tagged proteins with the ability to be used in multiple analyses of their respective analytes[48-50]. Upon development of reversible applications, researchers then began to focus on decreasing the bulkiness of SPR instruments in the aim of using SPR techniques in field analyses[51-55]. In particular, Naimushin *et al* developed a portable SPR immunosensor ideal for field use consisting of a multi-channel design and temperature control[54]. Mauriz *et al* also used a portable SPR biosensor to monitor the insecticide chlorpyrifos in ground, river, and drinking water samples down to 45 ngL^{-1} [52].

SPR Surface chemistry

SPR is unique in its ability to use sensor chips tailored to the analyte of interest by altering the surface chemistry of the SAM. For instance, SPR sensor chips can be functionalized with SAMs composed of planar polyethylene glycol/ carboxyl, linear polycarboxylate hydrogel, or carboxymethyl dextran[1]. A common surface manipulation scheme for these chips includes an EDC/ NHS protocol in which the EDC/NHS solution is used to activate the SAM. Ethanolamine is used to block any unoccupied space on the chip. The analyte sample is then injected and captured by the SAM[1]. Plain gold sensor chips can also be purchased and functionalized to tailor the analyte of interest.

EDC/NHS sensor chip chemistry has been used in the detection of Legionella pnemophila developed by Lin *et al*[56]. Lin *et al* immobilized anti-*L. pnemophila* (LPS) antibodies onto a SAM of MUA (11-mercaptoundecanoic acid) on a Au sensor chip. The SAM was activated by standard EDC/NHS protocol before the *L. pnemophila* antigen was injected. The system was able to detect the antigen as low as 10(1) CFU/ml[56]. Similar EDC/NHS manipulation was illustrated by Yu-Cheng *et al*[57]. Yu-Cheng *et al* used a SAM of MUA activated by EDC/NHS to detect BSA. Further, the sensitivity of the system was increased by modifying the sensor chip with cold plasma techniques[57]. Yu-Cheng *et al* was able to achieve a detection limit of $5ngL^{-1}$ BSA[57]. EDC/NHS protocol was also utilized by Xiao *et al* to detect phage T4[58]. *Escherichia coli* was immobilized onto a SAM of methiopropamine (MPA) activated by EDC/NHS. This system exhibited specific absorption of the phage T4 with a proportional response to various phage T4 concentrations[58].

SPR Applications

In addition to the ability to customize the surface of its sensor chips, SPR analysis is also praised for its sensitivity, label free system, minimal time requirement, small sample volume, and ability to regenerate the sensor surface[45, 59, 60]. SPR techniques have been used in various applications including medical analyses and food safety analyses[44, 61-64].

In relation to medical analyses, using SPR techniques to detect thrombin is a major area of research[44, 61, 62, 65, 66]. Mani *et al* for example used SPR techniques to detect thrombin in buffer and serum samples[61]. A bi-cell SPR spectrometer was used to immobilize a thrombin aptamer in preparation for thrombin analysis[61]. A detection limit of 25nM was achieved when the thrombin was in a Tris buffer solution. A detection limit of 50nM was achieved when the thrombin was in a serum solution[61]. Zheng *et al* also used SPR techniques to detect thrombin[44]. Zheng *et al* functionalized a gold sensor chip in a two step process in which MPA immobilization was followed by aptamer immobilization. Zheng *et al* examined a thrombin aptamer and an anti-thrombin aptamer. The thrombin aptamer successfully bound thrombin and resulted in a detection range of 5-1000nM. Further, when BSA was included in the thrombin solution, there was no significant change in SPR response illustrating efficient selectivity of the thrombin aptamer. The anti-thrombin aptamer did not result in thrombin binding[44]. Thus both, Mani *et al* and Zheng *et al* illustrate successful SPR systems for the detection of thrombin.

SPR techniques are also used in various food safety applications. Tran *et al* for instance used SPR analysis to detect a common food allergen, peanuts[63]. Arah1 protein was analyzed as an

indicator of peanut presence in a sample. Tran *et al* used aptamers selective for Arah1 and observed proportional SPR response to varying concentrations of Arah1 in both TGK buffer and candy bar samples. The aptamers were concluded to have a dissociation constant of 353 nM and the SPR system was deemed selective and sufficient for peanut allergen detection[63]. Another important aspect of food safety monitoring is the ability to detect food borne pathogens. Wang *et al* used SPR techniques to monitor *Escherichia coli* O157:H7 in food matrices of cucumbers and ground beef[64]. Five lectins were used as the bioreceptors to bind to *E. coli* O157:H7 within the SPR system. The limit of detection was observed at 3×10^3 cfu mL^{-1} as a result of the *T. vulgaris* lectin. Also, proportional responses were observed between *E. coli* O157:H7 concentrations and SPR responses. Thus, the SPR system was concluded to be an efficient and selective means to detect *E.coli* O157:H7 within complex food matrices[64].

PESTICIDES

Classes

Pesticides are used in numerous agricultural applications to mediate and prevent adverse effects from ecological pressures. The major categories of pesticides include insecticides, miticides, herbicides, fungicides, bactericides, and virucides. Each type of pesticide targets a unique ecological pressure. For example, insecticides and miticides target insects and mites respectively, fungicides target fungal spores or fungi, and herbicides target invasive plant species. Each type of pesticide can be further classified based on its mode of action, use, or activity. Insecticides, in particular, include organophosphates, carbamates, pyrethroids, neonicotinoids, and ryanoids. This paper will focus on organophosphate and neonicotinoid insecticides.

Organophosphates

Organophosphates (OP) are a class of insecticides that inhibit the hydrolysis of acetylcholine (ACh) by interfering with acetylcholinesterase (AChE)[67]. Prior to OP exposure, AChE degrades ACh into choline and acetic acid[68]. This degradation is a regulatory response to maintain proper ACh activity. ACh aids in the transmission of nerve impulses to effector cells and thus aids in the stimulation of nerve fibers or muscles[68]. Upon OP insecticide exposure, however, AChE is phosphorylated at its serine hydroxyl moiety and can no longer hydrolyze ACh. ACh in return continues to transmit nerve impulses and ultimately results in overstimulation and insect paralyzation[68].

OP insecticides account for 50% of insecticide sales worldwide[69]. The origin of OP insecticides dates back to the 20th century with its synthesis by Gerhard Schrader[70, 71]. Applications of OP insecticides include controlling illnesses such as yellow fever and malaria along with the control of agricultural pests[72]. Despite its acute toxicity to humans, OP insecticides have been correlated with various adverse health conditions including metabolic diseases, respiratory diseases, and neurological disorders such as diabetes, respiratory blockage, and Alzheimer's Disease respectively[73-76]. Thus, optimizing organophosphate insecticide detection mechanisms is vital to minimize the onset of these health conditions.

To directly monitor exposure to OP insecticides for instance, Okamura *et al* used GC-MS to detect urinary 3-methyl-4-nitrophenol (MNP), a biomarker for OP exposure, and p-nitrophenol (PNP), a metabolite of parathion[77]. The metabolites were monitored in occupational sprayers and

general workers over a summer and winter. The detection limit for MNP was observed to be 0.3 mu g/L and the detection limit for PNP was observed to be 0.5 mu g/L. The conclusion of the study found MNP concentrations to be much higher in the occupational sprayers in comparison to the general workers with a higher concentration observed in the summer. No significant difference in PNP concentration were observed between the two groups however. Okamura *et al* concluded the use of GC-MS as a sufficient and sensitive means to monitor OP biomarkers in humans[77].

Another means of detecting OP insecticides is to analyze possible residues on food commodities. Fuentes-Matus *et al* used liquid GC with a thermionic specific detector to detect malathion residues in mangos[78]. Malathion was applied to two varieties of mangos, Ataulfo and Atkins, at days 1, 30, and 60. Fuentes-Matus *et al* observed malathion in 75% of the Ataulfo samples and 95.6% of the Atkins samples[78]. OP residues have also been analyzed on other food commodities such as grapes and apples by Sinha *et al*[79]. Sinha *et al* used LC-MS/MS to test for 18 OP insecticides on red grapes, green grapes, and apples. The detection limit was observed at 0.002 ppm with recoveries of 97%. Imidacloprid, fenitrothion, and quinalphosin were observed on the red and green grapes while imidacloprid, quinalphos, triazophos, ethion, and acephate were observed on the apples[79].

Neonicotinoids

Neonicotinoids are a synthetic class of insecticides that target piercing-sucking pests such as aphids, whiteflies, and leafhoppers[80]. Neonicotinoids account for 11-15% of insecticide sales worldwide[80]. Its origin began in the 1970s with the discovery of 2-(dibromonitromethyl)-3-

methylpyridine by the Shell Development Company[81, 82]. Neonicotinoids are effective systemically in crops, meaning the insecticide travels throughout the entire crop upon application. Neonicotinoids act as ACh mimics which results in hyper-excitation and eventual insect paralyzation[83]. Neonicotinoids are advantageous because they are more selective towards the insect form of ACh over the mammalian form of ACh[83]. Hence, although neonicotinoids are known for their high level of toxicity towards piercing and sucking insects; neonicotinoids are less potent towards mammals. However, despite its lower toxicity level in humans, neonicotinoid detection is still an important area of research gaining much attention.

Xu *et al* for example recently developed a rapid immunoassay to detect imidacloprid and thiamethoxam from cucumber, tomato, lettuce, orange, and apple[84]. The immunoassay used nano gold-labeled monoclonal antibodies with conjugates of imidacloprid-BSA and Thiamethoxam-BSA as the test lines and goat anti-mouse IgG as the control line. The system was able to achieve a detection limit of 0.5 ng/mL for imidacloprid and 2 ng/mL for thiamethoxam[84]. Watanabe *et al* also analyzed food matrices for the presence of neonicotinoids[85]. Watanabe *et al* optimized ELISA methods to detect dinotefuran in carrot, green pepper, cabbage, spinach, Japanese mustard spinach, and leek. Approximately 100% recovery was achieved with all of the samples except for komatsuna. A detection limit of 0.06 to 0.12 mg/kg was achieved[85]. In addition, Seccia *et al* optimized HPLC with diode-array detection (DAD) techniques to detect acetamiprid, imidacloprid, thiacloprid, and thiamethoxam in bovine whole milk samples[86]. Seccia *et al* achieved recovery rates from 85.1 to 99.7%[86].

Chapter 2: Using Surface Plasmon Resonance to Quantify and Compare the Efficiency of Malathion-Selective Aptamers

ABSTRACT

This study utilizes Surface Plasmon Resonance techniques to compare the efficiency of two malathion-selective aptamers denoted as aptamers 6 and 7. Each aptamer was analyzed as a component of a mixed SAM consisting of EG_3 or MCH on a gold sensor chip. The efficiencies of each functionalized gold sensor chip containing aptamers 6 and 7 were compared by analyzing their responses to malathion solutions with concentrations of 250 µM, 100 µM, and 50 µM. The gold sensor chip functionalized off-line with aptamer 7 resulted in responses of 121.4 µRIU, 75.1 µRIU, and 59.3 µRIU to malathion solutions of 250 µM, 100 µM, and 50 µM respectively. The gold sensor chip functionalized off-line with aptamer 6 resulted in responses of 81.0 µRIU, 47.7 µRIU, and 40.5 µRIU to malathion solutions of 250 µM, 100 µM, and 50 µM respectively. Thus, aptamer 7 was responsible for a greater SPR response at each malathion concentration. Once the more efficient aptamer was concluded to be aptamer 7, the immobilization of aptamer 7 onto the plain gold sensor chip was quantified to be 20 µRIU. Further, the efficiency of aptamer 7 was also illustrated as malathion solutions of 200 µM, 400 µM, 600 µM, and 800 µM were injected onto a gold sensor chip functionalized on-line with a mixed SAM of aptamer 7 and MCH resulting in SPR responses of 39.1 µRIU, 76.3 µRIU, 130.8 µRIU, and 151.2 µRIU respectively.

INTRODUCTION

Being able to detect trace concentrations of insecticides is essential when analyzing food commodities for insecticide residue level compliancy with tolerances set by the EPA. Current methods for insecticide analysis include fluorescence spectroscopy, high performance liquid chromatography (HPLC), thin-layer chromatography (TLC), gas chromatography/ mass spectrometry (GC/MS), enzyme-linked immunosorbent assay (ELISA), and liquid chromatography/ mass spectrometry (LC/MS)[3, 34, 39, 45, 87-95]. Although these methods have been effective at trace analyte analysis with sufficient selectivity and sensitivity, these methods are time consuming, require extensive sample preparation, large sample volumes, expensive equipment, and lack real-time analysis[3, 34, 87, 90]. A concern with the ELISA method in particular is its inconsistency between batches and time required to produce antibodies[3]. Thus, researchers have begun to find alternative methods of trace analyte analysis such as Surface-Enhanced Raman Spectroscopy (SERS) to overcome these issues.

SERS is an emerging spectroscopic technique that can conduct trace analyte detection in real-time[3]. SERS increases the Raman signal of a molecule due to the amplification of surface plasmon resonance at the metal surface and chemisorption of the molecule's electrons at the metal surface[2, 16]. The enhancement factor due to SERS has been observed to range from 10^6 to 10^{15}. However, the intensity of this enhancement factor is dependent on the proximity of the analyte to the metal surface. Thus, many applications use aptamers as a means to capture and bring the analyte closer to the metal's surface for optimal SERS enhancement[17].

Aptamers are short sequences of DNA or RNA that are tailored to select specific molecules. Their selectivity arises from the SELEX (systematic evolution of ligands by exponential amplification) method in which a DNA library is put through a series of selection and amplification steps until aptamers of interest are isolated[81,82]. Because the SELEX process results in more than one efficient aptamer, however, further analysis can aid in selecting the best aptamer of interest. Surface plasmon resonance (SPR) is an analytical technique that can aid in the selection of the optimal aptamer.

SPR is an optical technique that measures the change in refractive index at the surface of a metal upon analyte binding[16]. The SPR phenomenon is attributed to analysis of the incident angle reflected from its prism. SPR is ideal for quantification of an aptamer's binding efficiency due to its sensitivity, small sample volume, and ability to conduct real-time analysis [16,18]. The aim of this study is to use SPR as an analytical tool to quantify the binding efficiency of two malathion-specific aptamers in an effort to aid in choosing the optimal aptamer for other applications. Further, SPR will be used to quantify the immobilization of the more efficient malathion-selective aptamer to the surface of a gold sensor chip. To assist in optimal stability of aptamer binding, a mixed SAM consisting of malathion-selective aptamer and triethylene glycol monoamine (EG_3) or 6-mercapto-1-hexanol (MCH) is used. These co-adsorbents minimize non-specific nitrogenous binding of the aptamers to the gold sensor chip surface.

EXPERIMENTAL

Materials

Reagents were used as received. 1-ethyl-3-(3-dimethylamino propyl) carbodiimide, hydrochloride (EDC) and N-hydroxysuccinimide (NHS) were received from Thermo Scientific (Waltham, MA). BSA and anti-BSA IgG were obtained from Sigma Aldrich (St. Louis, MO). A mixed SAM of 10% COOH-$(PEG)_6$-Alkanethiol/ 90% OH-$(PEG)_3$-Alkanthiol gold sensor chips were obtained from Reichert Technologies (Depew, NY). 6-mercapto-1-hexanol (MCH) was obtained from Sigma Aldrich (St. Louis, MO). Malathion 98% purity was obtained from Chem Service (West Chester, PA). Plain gold sensor chips were obtained from Reichert Technologies (Depew, NY). Type A immersion oil was obtained from Cargile (Cedar Grove, NJ). Triethylene glycol monoamine (EG_3) was obtained from Molbio Ultra (Boulder, CO). Aptamers were received from Integrated DNA Technologies, Inc. (Coralville, IA).

Buffers and Solutions

Phosphate buffered saline (PBS) was prepared with 0.05% Tween 20 to create PBST. The 0.2 M EDC/ 0.05 M NHS solution was prepared fresh in deionized water. 20 µg/mL BSA was prepared in 10 mM sodium acetate (pH 5.2). 1 M ethanolamine (pH 8.5) was prepared in deionized water. The anti-BSA IgG solutions of varying concentrations were prepared in PBST. 0.1 M PBS (pH 7.2) was prepared in deionized water. 1 M potassium phosphate buffer (PPB; pH 8) was prepared in deionized water. 100mM phosphoric acid (PPA) was prepared in deionized water. Malathion solutions were prepared in 0.1 M PBS.

Aptamer Development

The DNA aptamers utilized in this paper were designed by Bruno et al[96]. The aptamers were produced through the SELEX method. In this SELEX method, a DNA library of oligonucleotides is put through a series of selection and enrichment steps to isolate malathion-selective aptamers[96]. To isolate the malathion-selective aptamers, a PharmaLink affinity column was used to pass the DNA library through. The target aptamers were to bind to the immobilized malathion in the column. These specific aptamers were then eluted and put through a PCR enrichment step[96]. This process was repeated six more times until the aptamers of choice were isolated[40].

The aptamers isolated included two malathion-specific aptamers M25 Forward and M17 Forward, denoted as aptamer 6 and 7 respectively. Aptamer 6 has a DNA sequences of 5'-ThioMC6-ATCCGTCACACCTGCTCT-GGCCTTATGTAAAGCGTTGGG-TGGTGTTGGCTCCCGTAT and aptamer 7 has a DNA sequence of 5'-ThioMC6-ATCCGTCACACCTGCTCT-TATACACAATTGTTTTTCTCTTAACTTCTTGACTGC-TGGTGTTGGCTCCCGTAT.

SPR Efficiency Test

The SPR efficiency test was adopted from protocol by Reichert Technologies[1]. A gold sensor chip with a mixed SAM consisting of 10% COOH-$(PEG)_6$-Alkanethiol/ 90% OH-$(PEG)_3$-Alkanthiol was mounted onto the SR7000DC SPR spectrometer. PBST flowed over the chip overnight at 50 µL/min. PBST was injected several times, using a 500 µL loop, to ensure baseline stability. The flow rate was changed to 20 µL/min as the EDC/ NHS solution was

injected. EDC/ NHS activated the mixed SAM monolayer in preparation for BSA immobilization. 500 µL of the BSA solution was then injected onto the sample side of the flow cell for 10 mins.

An aliquot of 1 M ethanolamine was injected onto both the sample and reference sides of the flow cell for 10 mins to deactivate any functional groups from the mixed SAM not occupied by immobilized BSA. This was followed by a PBST injection. Non-bound BSA was removed by injecting a 20 mM HCl solution for 3 mins at 20 µL/ min. This was followed by a PBST injection. The following anti-BSA IgG solutions were then injected in duplicates for 3.5 mins followed by a 5 min dissociation: 160 µg/mL, 80 µg/mL, 40 µg/mL, 20 µg/mL, 10 µg/mL and 5 µg/mL. Between each anti-BSA IgG injection, 20 mM HCl was injected for 3 mins to regenerate the gold sensor chip surface.

Gold Sensor Chip Functionalization

The plain gold sensor chips were functionalized with the following two methods: functionalization of the sensor chip prior to SR7000DC mounting, denoted as off-line functionalization, and functionalization of the sensor chip within the parameters of the SR7000DC, denoted as on-line functionalization. Both methods were adopted from techniques in the literature[97].

Off-line functionalization of gold sensor chip

Two plain gold sensor chips were cleaned by rinsing with DI water, followed by an ethanol rinse, and concluded with a DI water rinse. The chips were then dried with a stream of nitrogen.

Aptamers 6 and 7 were thawed, vortexed briefly, and quickly centrifuged. An aliquot of 1 µM of each aptamer was created in 1 M K_2PO_4 (pH 8). Each gold sensor chip was saturated with a separate aptamer solution and allowed to sit for 2 hrs at room temperature covered in a small Petri dish. The functionalized sensor chips were then carefully rinsed with DI water and dried under a stream of nitrogen.

Each sensor chip was saturated with a solution of EG_3 in which 3 µL of EG_3 was combined with 1.2 mL of ethanol. The saturated chips stood at room temperature for 2 hrs covered in a Petri dish. Figure 1 illustrates the surface chemistry of each gold sensor chip functionalized off-line with aptamers 6 and 7. The gold sensor chip with the mixed SAM containing aptamer 6 functionalized off-line was analyzed first. The gold sensor chip functionalized off-line with aptamer 7 was stored at 4°C until needed. The gold sensor chip with aptamer 6 was mounted onto the SR7000DC using Immersion Oil Type A. The tubing was connected so that the running buffer, 0.1 M PBS (PH 7.2), ran through the sample side of the flow cell only. 0.1 M PBS ran at 100 µL/ min for approximately 10 mins before data collection began. Once data collection began, the buffer was allowed to run over the sensor chip overnight at 25 µL/min. The flow rate was then changed to 50 µL/min.

(a)

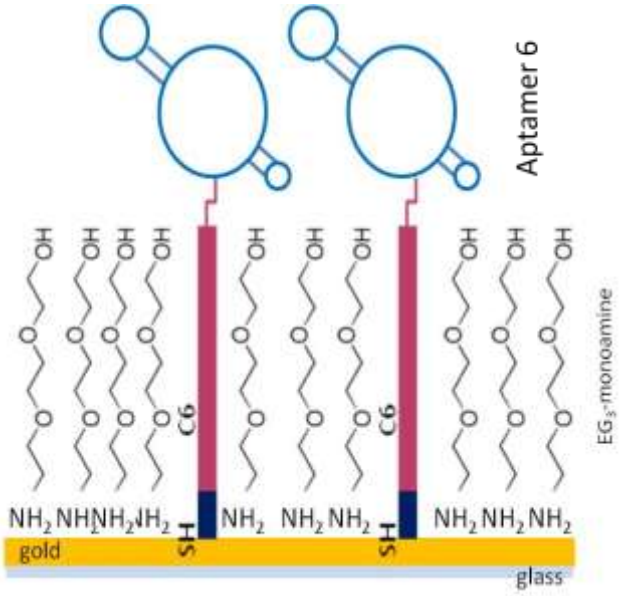

(b)

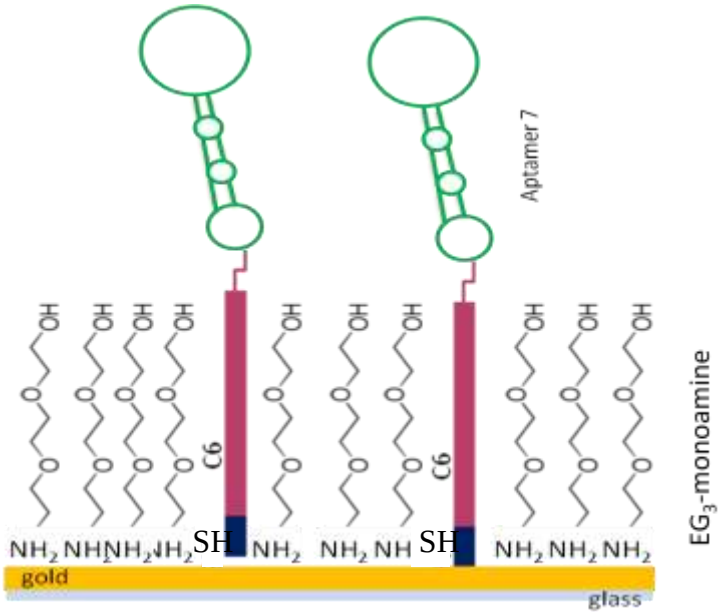

Figure 1. (a) Gold sensor chip with a mixed SAM of aptamer 6 and EG_3 monoamine in a 1:10 ratio respectively. (b) Gold sensor chip with a mixed SAM of aptamer 7 and EG_3 monoamine in a 1:10 ratio respectively. The thiol caps on both aptamers allow the aptamers to bind to the gold sensor chip surface. The 6-carbon (C6) spacers on the aptamers aid in maintaining proper aptamer orientation on the gold sensor chip surface. EG_3 monoamine minimizes non-specific binding of the aptamers to the gold sensor chip surface. Both gold sensor chips were functionalized off-line.

The sample loop was cleaned and the PPA regeneration solution was injected as previously described. Next, the following concentrations of malathion were injected at a flow rate of 50 µL/min for 3.5 mins and dissociated for 5 mins: 250 µM, 100 µM, and 50 µM. Between each malathion injection, the surface of the sensor chip was regenerated. This protocol was then repeated with the sensor chip functionalized with aptamer 7 off-line.

On-line functionalization of gold sensor chip

A plain gold sensor chip was mounted onto the SR7000DC using Immersion Oil Type A. The 0.1 M PBS running buffer was allowed to flow over the sensor chip for 10 mins before data collection began. The running buffer was then allowed to stabilize overnight by running over the sensor chip at 25 µL/ min. The next day the tubing was arranged so the buffer flowed over the sample side of the flow cell only. The flow rate was changed to 20 µL/min. A mixed SAM was created in a two step process by first injecting 500 µL of a 1 µM aptamer 7 solution in 1 M PPB (pH 8) for 3.5 hrs at 20 µL/min followed by a 30 min dissociation. Then 500 µL of a MCH solution (50 µL MCH stock and 450 µL of 1 M PPB (pH 8)) was injected for 1.5 hrs at 20 µL/min followed by a 30 min dissociation.

The tubing was then reconnected so the running buffer flowed over the sample and reference side of the flow cell. The flow rate was changed to 50 µL/ min. The sample loop was cleaned and 100 mM PPA was injected for 3 mins to remove any non-bound MCH or aptamers. Figure 2 illustrates the surface chemistry of the gold sensor chip functionalized on-line. The sample loop was cleaned as previously stated. The following concentrations of malathion were injected for 3.5 mins then allowed to dissociate for an additional 5 mins: 200 µM, 400 µM, 600 µM, and 800

µM. In between each malathion injection, 100 mM PPA was injected for 3 mins and allowed to dissociate for an additional 3 mins. Malathion was also injected onto a plain gold sensor chip at 200 µM, 400 µM, 600 µM, and 800 µM to analyze its response to the surface without aptamers.

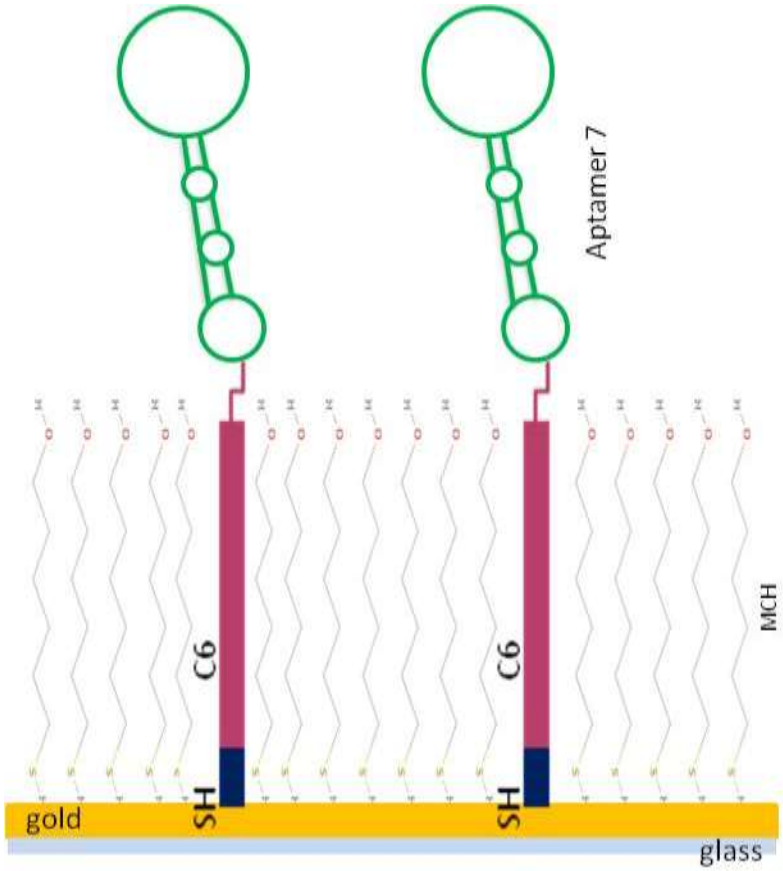

Figure 2. Gold sensor chip illustrating a mixed SAM of aptamer 7 and MCH in a 1:10 ratio respectively. The co-absorbent MCH assists in minimizing non-specific immobilization of the aptamer onto the gold sensor chip surface. The thiol group allows the aptamer to immobilize on the metal surface while the 6 carbon spacer (C6) aids in the maintenance of proper aptamer orientation. This gold sensor chip was functionalized on-line.

RESULTS AND DISCUSSION

This study proposes the use of SPR techniques to compare the efficiency of aptamers 6 and 7 in binding malathion along with the quantification of the immobilization of the more efficient aptamer onto a gold sensor chip surface. To directly compare aptamers 6 and 7, off-line functionalization techniques from the literature were used to functionalize plain gold sensor chips[97]. On-line functionalization techniques were used to compare the magnitude of SPR response upon malathion binding between aptamers 6 and 7 along with analyzing malathion interactions with a gold sensor chip functionalized with the more efficient aptamer.

Efficiency of the SPR7000DC System

Initial experiments were conducted to analyze the efficiency of the SPR system to achieve expected results comparable to a standard manipulation of gold sensor chips containing a mixed SAM of 10% COOH-$(PEG)_6$-Alkanethiol/ 90% OH-$(PEG)_3$-Alkanthiol. BSA versus anti-BSA IgG analysis was conducted following protocol from Reichert using the SPR7000DC[1]. The aim of this test was to efficiently immobilize BSA onto the mixed SAM gold sensor chip followed by analysis of anti-BSA IgG injections. The resulting sensogram should exhibit similar SPR responses to the expected sensogram illustrated by Reichert[1].

Figure 3 illustrates each step observed upon injection of an aliquot of anti-BSA IgG onto the mixed SAM with immobilized BSA. Figure 4 illustrates the resulting sensorgram of each anti-BSA IgG injections at various concentrations which parallels the expected results displayed in the literature[1]. The sensorgram shows a decrease in the change of μRIU with a decrease in anti-BSA IgG concentration. Each concentration shows characteristic responses at its injection,

dissociation, and surface regeneration steps. Also, after each injection, the baseline of the running buffer returns to a consistent response. Further, both the resulting sensorgram and reports from the literature exhibit SPR responses of 750 µRIU, 500 µRIU, 250 µRIU, 150 µRIU, and <100 µRIU at anti-BSA IgG concentrations of 80 µg/mL, 40 µg/mL, 20 µg/mL, 10 µg/mL, and 5 µg/mL respectively[1]. Because these characteristics match the expected results from Reichert Technologies, the SR7000DC was concluded to be efficient to carry out further SPR measurements.

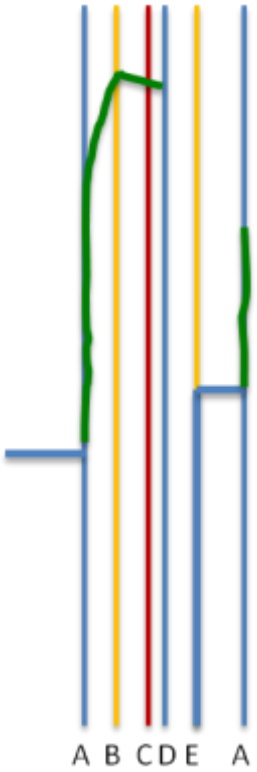

Figure 3. Sensorgram defining each step observed upon injection of an aliquot of anti-BSA IgG onto a mixed SAM of 10% COOH- $(PEG)_6$- Alkanethiol/ 90% OH-$(PEG)_3$- Alkanethiol with immobilized BSA. Step A starts the injection of the anti-BSA IgG aliquot, step B is the start of the dissociation, step C is the end of the dissociation, step D begins the surface regeneration, step E is the end of the surface regeneration, and step A starts the injection of the next aliquot of anti-BSA IgG.

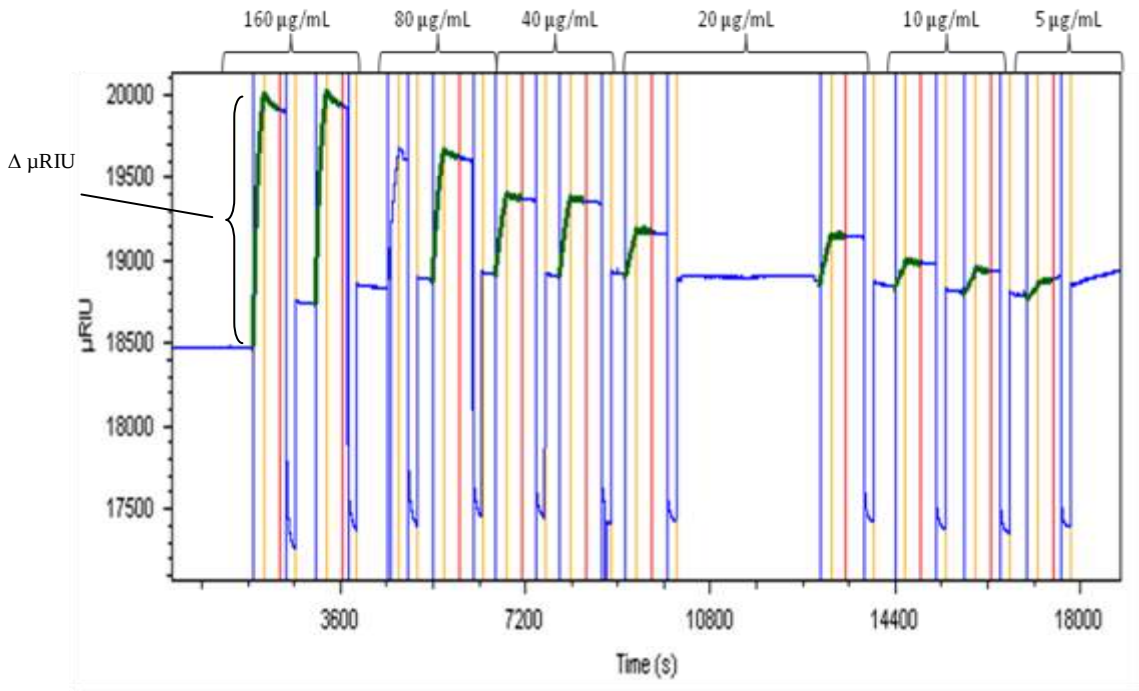

Figure 4. Sensorgram of anti-BSA IgG injections onto a mixed SAM of 10% COOH-$(PEG)_6$- Alkanethiol/ 90% OH-$(PEG)_3$- Alkanethiol with immobilized BSA. From left to right each pair of peaks represents anti-BSA IgG injections with concentrations of 160 µg/mL, 80 µg/mL, 40 µg/mL, 20 µg/mL, 10 µg/mL, and 5 µg/mL, respectively. The consistency of the SPR response at each concentration was compared to standard results from the literature[1]. A SPR response of approximately 1250 µRIU was observed at 160 µg/mL anti-BSA IgG from the above sensorgram in comparison to a SPR response of approximately 1000 µRIU from the literature[1]. Both the above sensorgram and standard results exhibited SPR responses of approximately 750 µRIU, 500 µRIU, 250 µRIU, 150 µRIU, and <100 µRIU at anti-BSA IgG concentrations of 80 µg/mL, 40 µg/mL, 20 µg/mL, 10 µg/mL, and 5 µg/mL respectively. The SPR was deemed efficient because of these similar responses at each anti-BSA IgG concentration.

Analysis of Functionalized Gold Sensor Chips

Off-line techniques were used to functionalize plain gold sensor chips with aptamers 6 and 7. Each aptamer contains a thiol cap along with a 6-carbon (C6) spacer at their 5' end. The thiol cap allows the aptamers to bind to the gold sensor chip surface. The C6 spacer aids in the extension of the aptamers above the surface of the gold sensor chip. The C6 spacers along with EG3 and MCH co-adsorbents aid in minimizing non-specific aptamer binding to the gold sensor chip surface and decrease inconsistencies of aptamer orientation.

Once the plain gold chips were functionalized off-line with a mixed SAM of their respective aptamer and EG_3, they were mounted onto the SPR7000DC for further analysis. Figure 5 (a) illustrates SPR responses of 81.0 µRIU, 47.7 µRIU, and 40.5 µRIU at malathion concentrations of 250 µM, 100 µM, and 50 µM respectively from the gold sensor chip functionalized with aptamer 6 off-line. The sensorgram exhibits characteristic injection and dissociation; thus, showing successful binding of malathion by aptamer 6. The change in µRIU decreases with a decrease in malathion concentration.

Figure 5 (b) illustrates SPR responses of 121.4 µRIU, 75.1 µRIU, and 59.3 µRIU at malathion concentrations of 250 µM, 100 µM, and 50 µM respectively from the gold sensor chip functionalized with aptamer 7 off-line. This sensorgram also shows standard injection, dissociation, and surface regeneration chemistry; thus illustrating successful capture of malathion by aptamer 7. The change in µRIU decreases with a decrease in malathion concentration. When comparing aptamers 6 and 7, the overall SPR response at each malathion concentration is greater from the chip functionalized with aptamer 7 off-line. Thus, although both aptamers can be

concluded to be efficient at binding malathion, aptamer 7 has a greater magnitude in response. Figure 6 shows the resulting calibration curves from plotting the malathion concentrations with their respective μRIU response from each sensor chip functionalized off-line. Linear regression analysis reveals a slope of 0.31008 for aptamer 7 and 0.207 for aptamer 6 which further illustrates a larger SPR response for aptamer 7 at the various malathion concentrations.

(a)

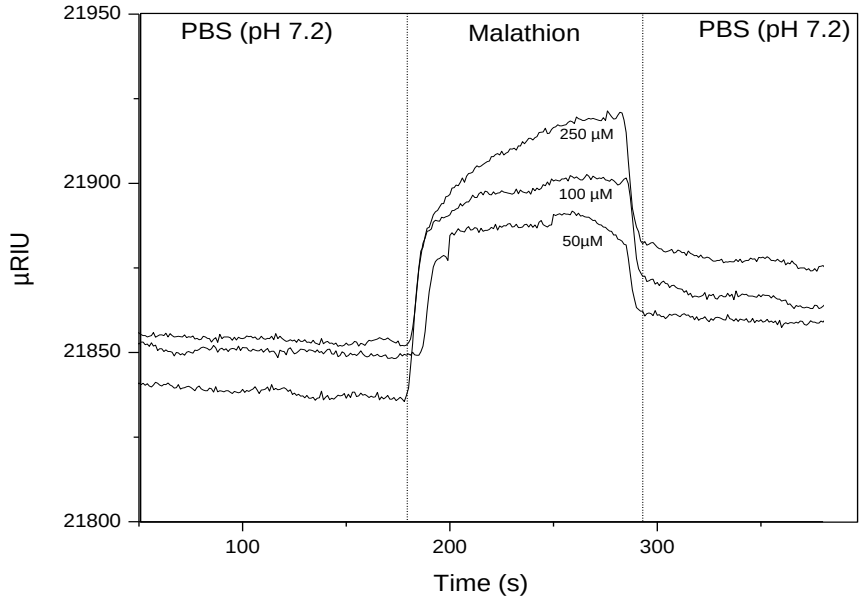

(b)

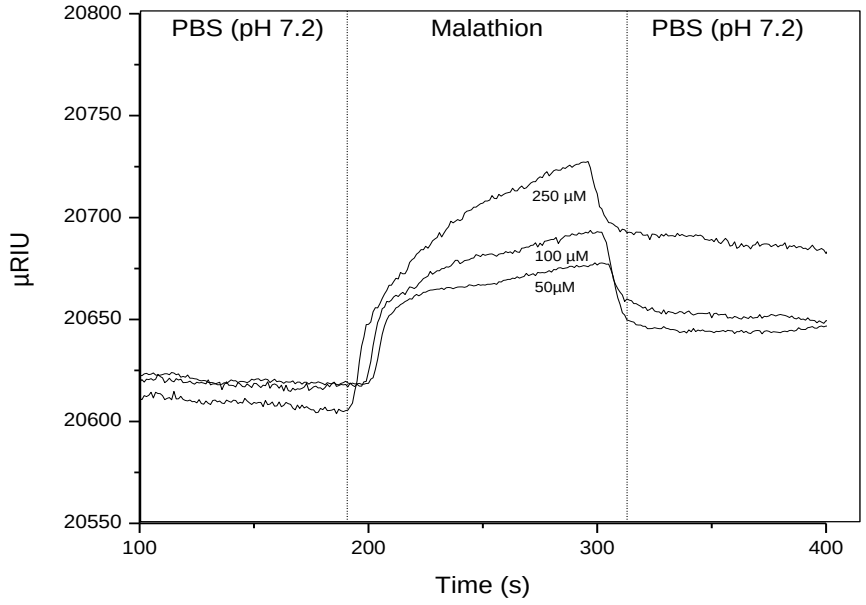

Figure 5. (a) Sensorgram of malathion solutions injected onto a gold sensor chip functionalized off-line with a mixed SAM of aptamer 6 and EG_3 in a 1:10 ratio respectively. A SPR response of 81.0 µRIU, 47.7 µRIU, and 40.5 µRIU was observed at malathion solutions of 250 µM, 100 µM, and 50 µM respectively. (b) Sensorgram of malathion solutions injected onto a gold sensor chip functionalized off-line with a mixed SAM of aptamer 7 and EG_3 in a 1:10 ratio respectively. A SPR response of 121.4 µRIU, 75.1 µRIU, and 59.3 µRIU was observed at malathion solutions of 250 µM, 100 µM, and 50 µM respectively.

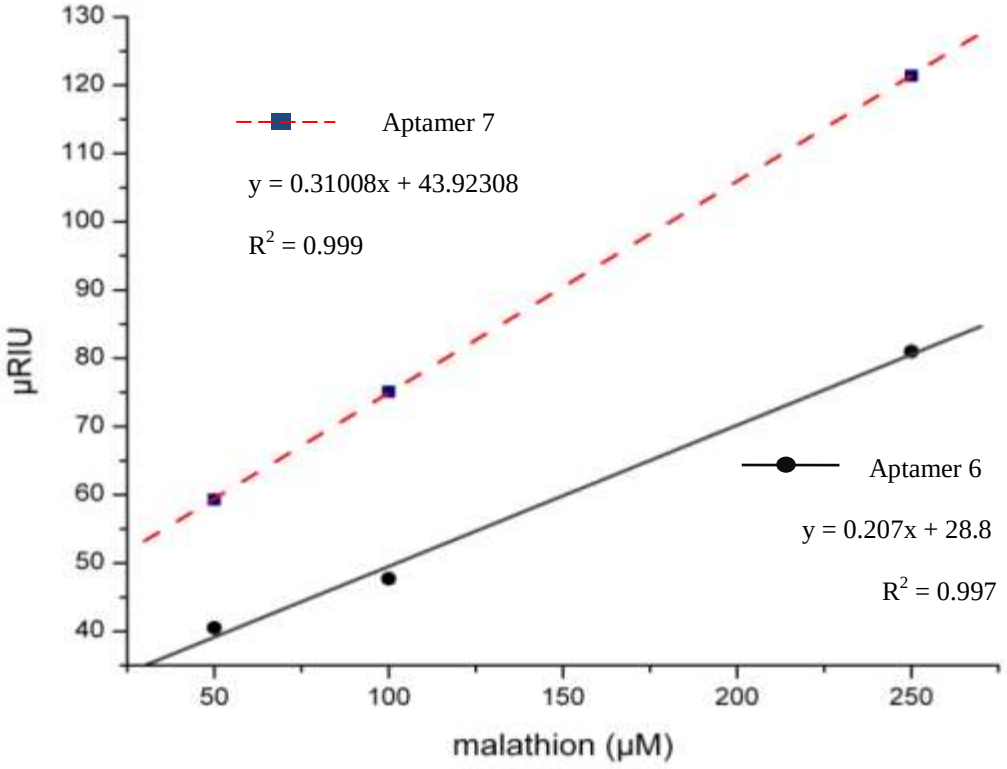

Figure 6. Calibration curves created by plotting the SPR response observed at each malathion concentration for the gold sensor chip functionalized with aptamer 6 off-line and the gold sensor chip functionalized with aptamer 7 off-line. Aptamer 6 resulted in a slope of 0.207 while aptamer 7 resulted in a slope of 0.31008. The larger slope illustrates an overall greater SPR response at each malathion concentration for the gold sensor chip functionalized with aptamer 7 off-line.

Figure 7 illustrates successful immobilization of aptamer 7 onto the gold sensor chip surface. The sensorgram exhibits proper injection, dissociation, and surface regeneration chemistry in which a response of 20 µRIU is observed. Thus, one can conclude that aptamer 7 has efficiently immobilized onto the gold sensor surface. Figure 8 illustrates a SPR response of 39.1 µRIU, 76.3 µRIU, 130.8 µRIU, and 151.2 µRIU to malathion solutions of 200 µM, 400 µM, 600 µM, and 800 µM respectively from the gold sensor chip with a mixed SAM of aptamer 7 and MCH functionalized on-line. Thus, a proportional relationship between intensity of response and malathion concentration is observed.

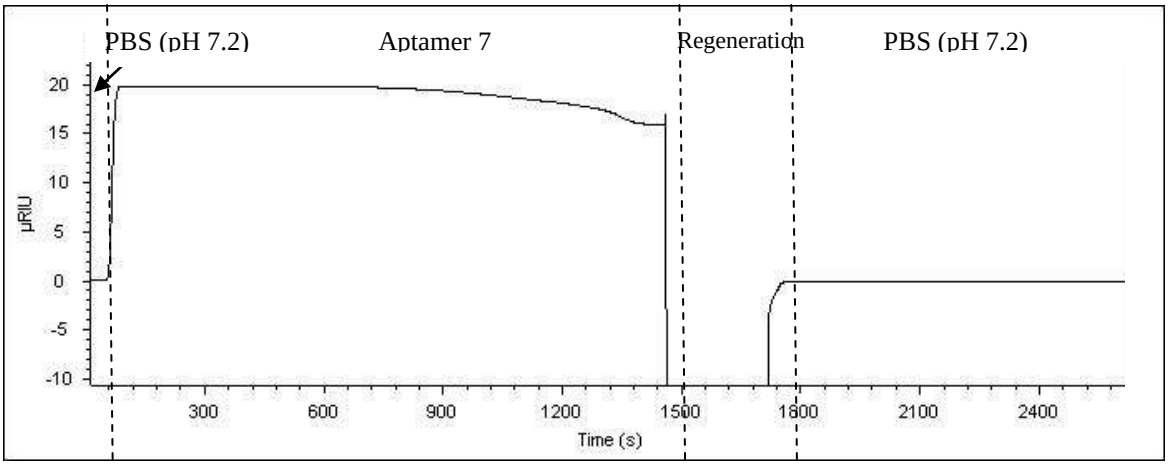

Figure 7. Sensorgram illustrating the successful immobilization of aptamer 7 onto a plain gold sensor chip. The immobilization of aptamer 7 results in a SPR response of 20 µRIU.

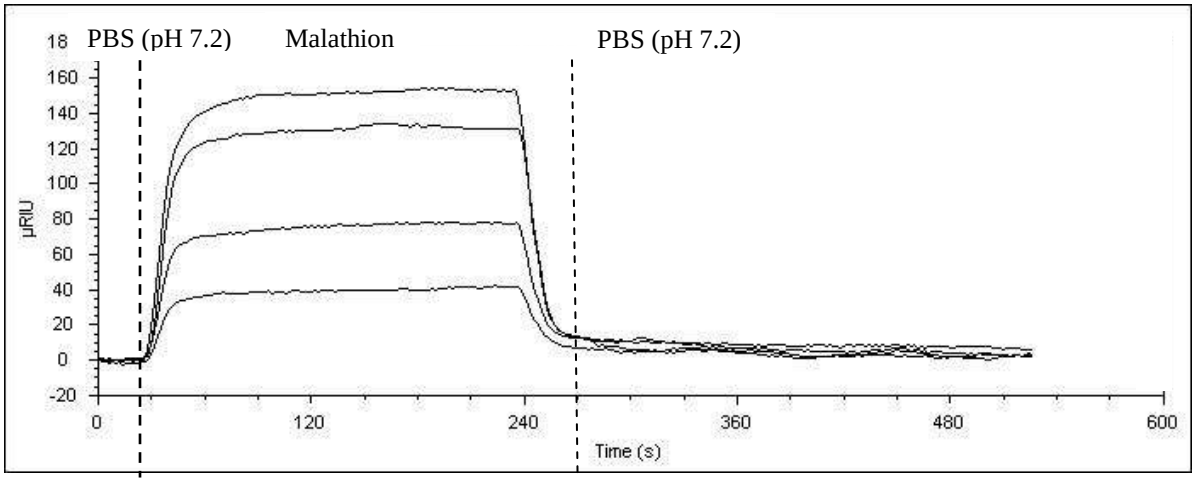

Figure 8. **Sensorgram of malathion injections onto a gold sensor chip with a mixed SAM of aptamer 7 and MCH functionalized on-line. Sensorgram illustrates proper injection and dissociation chemistry. A proportional relationship is illustrated between SPR response and malathion concentration with a SPR response of 39.1 µRIU, 76.3 µRIU, 130.8 µRIU, and 151.2 µRIU to malathion solutions of 200 µM, 400 µM, 600 µM, and 800 µM respectively.**

To further confirm these results one should examine the ability of non-malathion specific aptamers to cause a change in the refractive index of the gold sensor chip surface upon malathion injection. One may also analyze the ability of the malathion-specific aptamers to select malathion within a complex sample matrix. An issue that arose with the technique included possible leaching of aptamers to the reference side of the flow cell. This issue may be overcome with a longer injection time for the aptamer or the use of a slower flow rate upon aptamer immobilization.

CONCLUSIONS

This study presents a SPR technique that efficiently quantifies the ability of two aptamers to bind malathion and quantifies the immobilization of aptamer 7 onto a gold sensor chip surface. The technique illustrates the varying ability of aptamers to select malathion by comparing the degrees of changes in μRIU. Although both aptamers 6 and 7 are shown to bind malathion, aptamer 7 has a greater affinity for malathion shown by its larger overall SPR response at each concentration of malathion. This SPR technique also quantifies the immobilization of aptamer 7 onto a gold sensor chip surface. These findings lend credence to literature applications that use aptamer 7 as a means to increase the SERS signal of malathion[40]. Although several malathion-selective aptamers are available, aptamer 7 has shown to be more efficient in this case. As more applications begin to use aptamers as diagnostic tools, SPR techniques can be used to optimize aptamer selections.

ACKNOWLEDGEMENTS

The author would like to thank Dr. Mary Murphy and Thomas Ryan from Reichert Technologies for assistance with the SR7000DC along with Dr. Cameron Bardliving for assistance with data analysis. The author acknowledges the financial support received from the United States Department of Agriculture (Grant 2009-35603-05066).

Chapter 3: Detection and Quantification of Common Insecticides in Apples Using Surface-Enhanced Raman Spectroscopy

ABSTRACT

Using Surface Enhanced Raman Spectroscopy (SERS) as an analytical tool to detect trace analytes is emerging as an important detection method that is surpassing traditional methods of analyte detection. This study presents an effective method for the analysis of common insecticides thiamethoxam, acetamiprid, chlorpyrifos, phosmet, and thiaclorpid using Surface Enhanced Raman Diagnostic Membranes (SER-DM^{TM}). Each calibration curve generated exhibited efficient correlation with R^2 values greater than 0.94. The calibration curves were then translated into tools for real-world sample analysis. Apple samples were analyzed for insecticide residues using the SER-DM^{TM} and the generated calibration curves were applied to quantify the presence of the residues. Analysis of the apple rinsates by the proposed methodology revealed the presence of peaks matching with chlorpyrifos and thiacloprid. The calibration curves were used to conclude the possible detection of chlorpyrifos and thiacloprid in concentrations of 1.1 ppb and 12.4 ppb respectively. These observed values were both below the EPA insecticide residue tolerance levels for apples.

INTRODUCTION

Insecticides are used on numerous food crops to optimize yield from harvest by decreasing the effects of agricultural pests and can be observed in trace quantities on food products in the marketplace[87]. Insecticides are classified into classes according to their different modes of action, use, or activity. Organophosphate and neonicotinoid insecticides for example generally act by over stimulation of an insect's nervous system which ultimately leads to insect death. Despite their effectiveness towards agricultural pests, chronic exposure to certain insecticides has shown to have potentially adverse effects in humans. These effects include problems with the central nervous system, respiratory system, and cardiovascular system[98, 99]. To maintain a safe food supply, the EPA sets tolerances for insecticide residues in sub-micro molar concentrations for various commodities. Thus, being able to quantify trace concentrations of insecticides is important when diagnosing the safety of such food commodities.

In order to meet these needs of trace insecticide detection, analytical scientists have traditionally used GC-MS, MS, LC-MS, and ELISA methods[91-95]. Although these methodologies are reliable and sensitive they require extensive sample preparation, large sample volumes, and lack real-time analysis ability[3, 34, 87, 90]. To overcome these issues, many researchers have turned to Surface-Enhanced Raman Spectroscopy (SERS) as a means to detect trace analytes in real time[2]. SERS is a vibrational spectroscopic technique that enhances the Raman signal of a molecule by chemisorption of the molecule to a metal surface. The enhancement factors are contributed by a chemical enhancement and an electromagnetic enhancement[2].

SERS substrates vary in nature, size, and shape and can range from Ag or Au nanorods, nanospheres, or nanogaps to nanoparticles arranged on polymer spheres or films[2, 42, 97]. Surface Enhanced Raman Diagnostic Membranes (SER-DM™) in particular are a novel SERS substrate for rapid trace analyte detection developed by iFyber (Ithaca, NY). These membranes are ideal for trace insecticide residue analysis due to their absorbent nature, custom shape, gold coating, and non-rigid structure[42]. This study proposes the use of a novel SERS substrate in the form of SER-DM™ to create calibration curves of common insecticide active ingredients that can be used for insecticide residue analysis.

EXPERIMENTAL

Materials

Reagents were used as received. Active ingredients thiamethoxam, acetamiprid, chlorpyrifos, phosmet, and thiacloprid were received from Sigma Aldrich (St. Louis, MO). Commercial formulations of insecticides Lorsban 75WG, Actara 25WG, Imidan 70W, Assail 30SG, and Calypso 4F were obtained from the New York State Agricultural Experiment Station (Geneva, NY). SER-DM™ were obtained from iFyber, LLC (Ithaca, NY). Apples were purchased from a local supermarket, January 2013 (Ithaca, NY). NERL reagent grade water was obtained from Thermo Scientific (Waltham, MA).

SERS Measurements

Active Ingredients versus Commercial Formulations

An aliquot of each active ingredient and commercial formulation was allowed to incubate with the SER-DM™ for 48 hrs at room temperature with consistent rocking in glass vials. Table 1

lists the composition of each commercial formulation. The membranes were then carefully placed onto glass slides by adherence with 2-sided tape. SERS signals of the solutions were captured using a hand-held spectrometer from iFyber (Ithaca, NY). The parameters used included 68 mW laser power, rastering, 1 s integration time, and an average of 5 captures per sample. The data was analyzed with Peak Data Acquisition Software and Grams AI 8.0 Spectroscopy Software.

Calibration curves were developed for thiamethoxam, acetamiprid, chlorpyrifos, phosmet, and thiacloprid. An aliquot of each active ingredient at various concentrations were incubated, in triplicates, with the SER-DM^{TM} for 48 hrs at room temperature with consistent shaking in glass vials. The membranes were then carefully placed onto glass slides. SERS signals of the solutions were captured using a hand held spectrometer from iFyber (Ithaca, NY). The parameters utilized included 67 mW laser power, rastering, 1 s integration time, and an average of 5 captures per sample. A characteristic peak was then defined for each insecticide.

Table 1. Composition of each commercial formulation in relation to its makeup of active ingredient. An aliquot of each commercial formulation and its active ingredient was incubated with triplicate samples of SER-DM for 48 hrs for comparison of SERS spectra between the commercial formulations and active ingredients.

Commercial Formulation	Composition
Actara 25WG	25.0 % thiamethoxam; 75.0 % other ingredients
Assail 30SG	30.0 % acetamiprid; 70.0 % other ingredients
Calypso 4F	40.4 % thiacloprid; 59.6 % inert ingredients
Imidan 70W	70.0 % phosmet; 30.0 % other ingredients
Lorsban 75WG	75.0 % chlorpyrifos; 25.0 % other ingredients

Calibration curves were created by plotting the various concentrations of active ingredients versus their respective intensities at a characteristic peak, as an average of the triplicate samples. The calibration curves were developed using Origin Pro 7.5 software.

Apple Analysis

Each of the 3 apples was rinsed with deionized water for 10 s. The entire volume of rinsate was collected and stirred for 5 mins to evenly distribute any residues in the sample. SER-DM^{TM} were then incubated with 1mL of each sample for 48 hrs at room temperature with consistent shaking in glass vials. The membranes were then placed onto glass slides before spectral acquisition. The parameters used included 68 mW laser power, rastering, 1 s integration time, and an average of 5 captures per sample. The data was analyzed with Peak Data Acquisition Software and Grams AI 8.0 Spectroscopy Software.

RESULTS AND DISCUSSION

Detection of Active Ingredients within Commercial Formulations

To examine the ability to detect the active ingredients within complex matrices of the commercial formulations, SERS spectra of each active ingredient and commercial formulation were obtained using SER-DM^{TM} and a hand-held spectrometer from iFyber, LLC. Figures 9 to 13 illustrate the spectra for each active ingredient and its commercial formulation obtained using the conditions described in the experimental section. Green circles represent peaks between each spectra pair with matching wave numbers. Yellow circles represent similar peak pairs that have wave numbers within 5 cm^{-1} of each other. Actara 25WG and its active ingredient thiamethoxam for instance share an identical peak at 992.2 cm^{-1}. However, Actara 25WG and thiamethoxam have peaks that are similar but not identical at 2131.2 cm^{-1} and 2127.6 cm^{-1} respectively. These

slight differences in wave numbers may represent the same vibrational mode transits, however small differences in the orientation of the absorbed molecule may generate differences in the spectra. Each commercial formulation exhibits numerous identical and similar peak wave numbers as its active ingredient. Table 2 summarizes the percentage of commercial formulation peaks that have identical or similar wave numbers to its active ingredient. 73.91% of Imidan 70W's peaks for example are identical or similar to the wave numbers observed for phosmet. 46.67% of Calypso 4F's peaks are identical or similar to the wave numbers of its active ingredient thiacloprid. This data successfully illustrates the ability of SER-DM^{TM} to detect active ingredients within the complex matrix of their commercial formulations.

Standard Curve Analysis

SER-DM^{TM} were used to examine SERS signals of the active ingredients at various concentrations for the generation of calibration curves. Upon acquisition of the SERS spectra, a characteristic peak was chosen for each active ingredient. Several aspects taken into account when choosing the characteristic peak included SERS data from the reagent grade water, the intensity of the peak, commonality of the peak in other insecticides, and defined characteristic peak wave numbers from the literature. Also taken into account was the chemical structure of each active ingredient shown in Table 3 because standard functional group assignments from SERS spectra exhibit particular wave numbers (cm^{-1}). The characteristic peaks, listed in Table 4, illustrated good resolution, high intensity, and proportional presence over several concentrations. Further, the vibrational coordinates compiled from the literature for the major peaks of each active ingredient are listed in Table 5[100-102]. These coordinates illustrate how the chemical structure of each active ingredient relates to the bands on their spectra. For example, peak

1006cm^{-1} in phosmet represents asymmetric P-O-C deformation vibration. After characteristic peaks were identified for each active ingredient, calibration curves were created by plotting the different concentrations of the active ingredients versus their respective intensities, as an average of the triplicate samples.

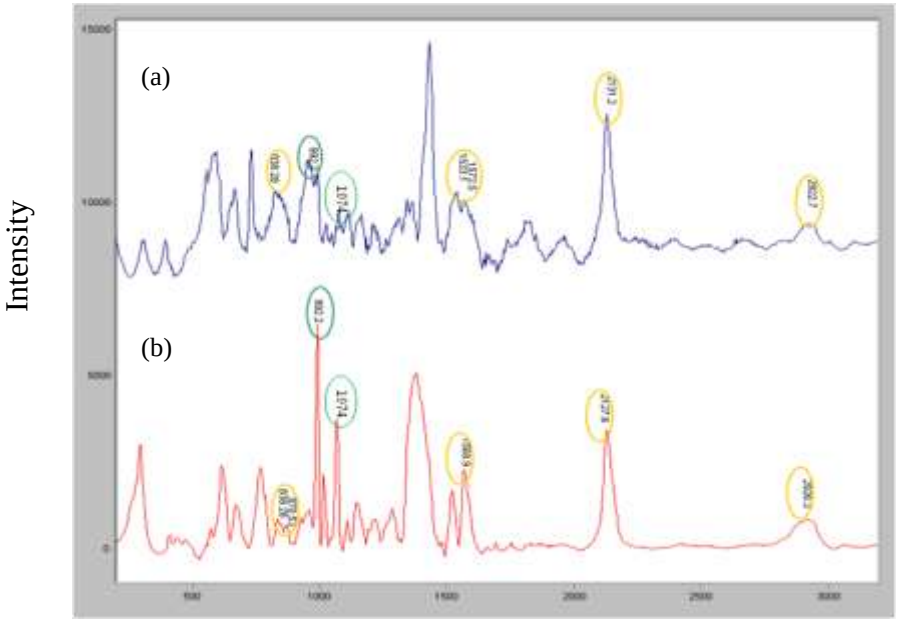

Figure 9. Identical peak observed at 992.2 cm^{-1} and 1074cm^{-1} between (a) sample of Actara 25WG commercial formulation composed of 25.0% thiamethoxam and (b) 500 µM thiamethoxam solution. Similar peaks within 5 cm^{-1} illustrated by yellow circles.

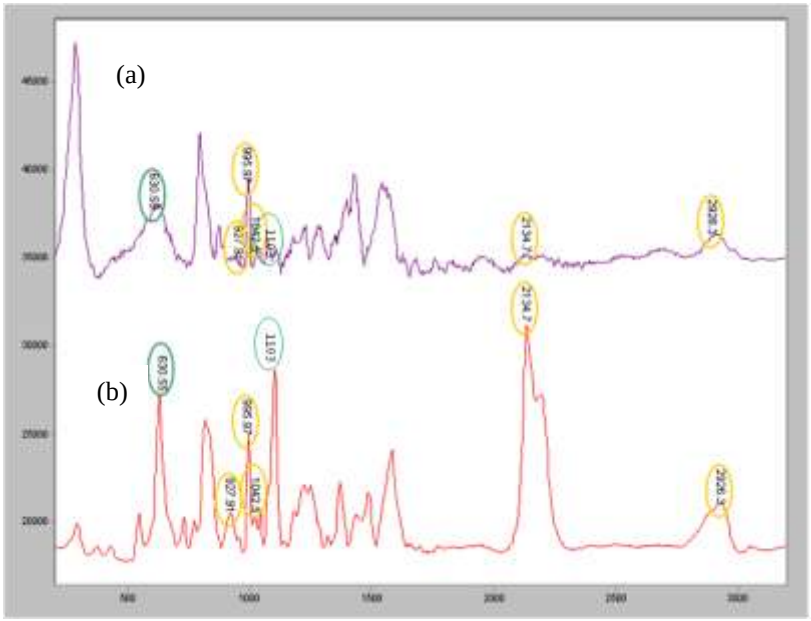

Figure 10. Identical peak observed at 630.55 cm^{-1} and 1103cm^{-1} between (a) sample of Assail 30SG commercial formulation composed of 30.0% acetamiprid and (b) 500 µM acetamiprid solution. Similar peaks within 5 cm illustrated by yellow

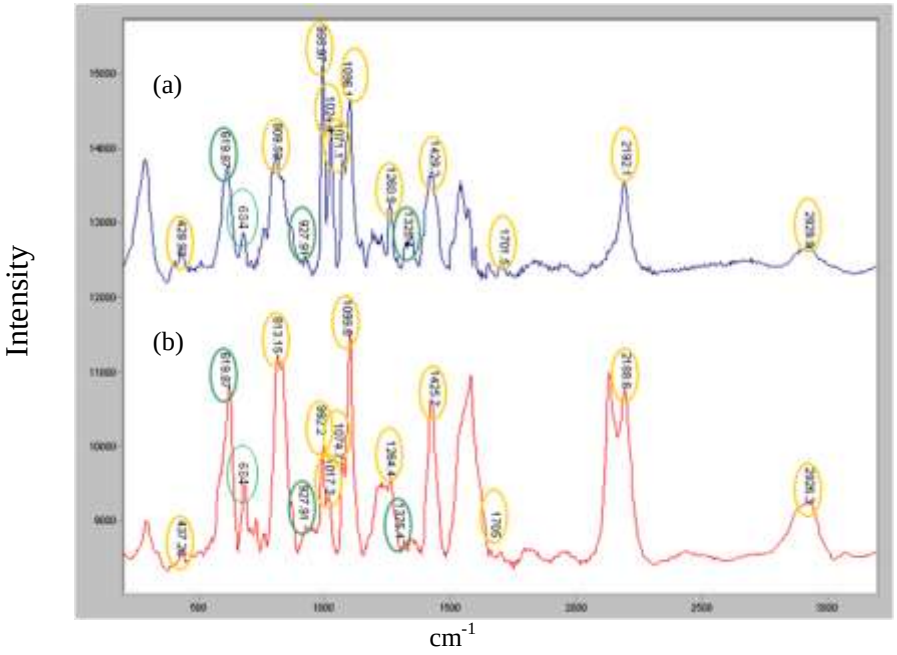

Figure 11. Identical peaks at 619.87 cm^{-1}, 684.0cm^{-1}, 927.91 cm^{-1}, and 1325.4 cm^{-1} between (a) Calypso 4F sample composed of 40.4% thiacloprid and (b) 500 µM thiacloprid solution. Similar peaks within 5 cm between the two spectra exhibited by yellow circles.

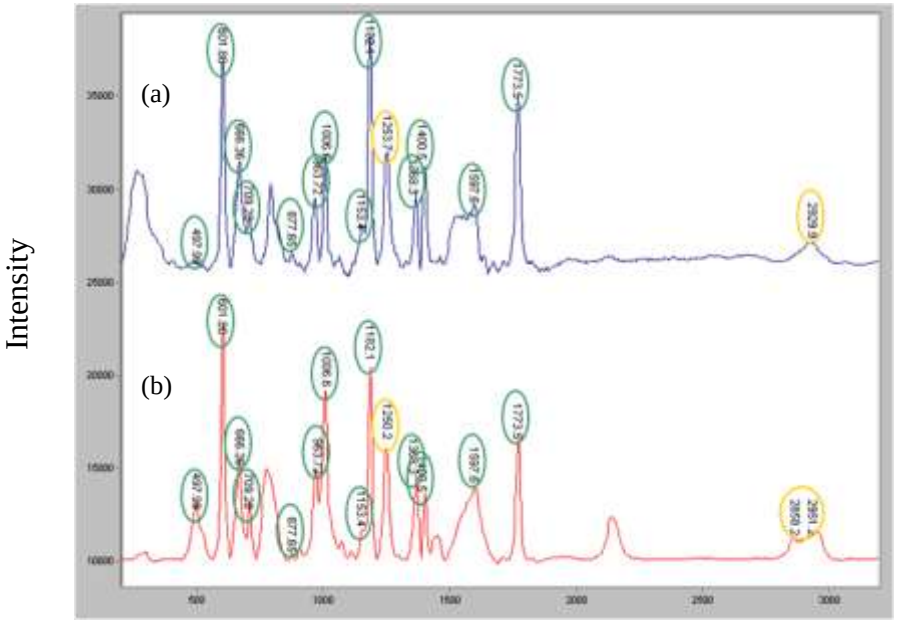

Figure 12. Identical peaks observed at 497.99cm^{-1}, 601.86cm^{-1}, 666.36cm^{-1}, 709.20cm^{-1}, 877.65cm^{-1}, 963.72cm^{-1}, 1006.6cm^{-1}, 1153.4cm^{-1}, 1182.1cm^{-1}, 1368.3cm^{-1}, 1400.5cm^{-1}, 1597.6cm^{-1}, and 1773.5cm^{-1} between (a) Imidan 70W sample composed of 70.0% phosmet and (b) a 70 µM phosmet solution. Similar peaks between the two samples within 5 cm are illustrated by yellow circles.

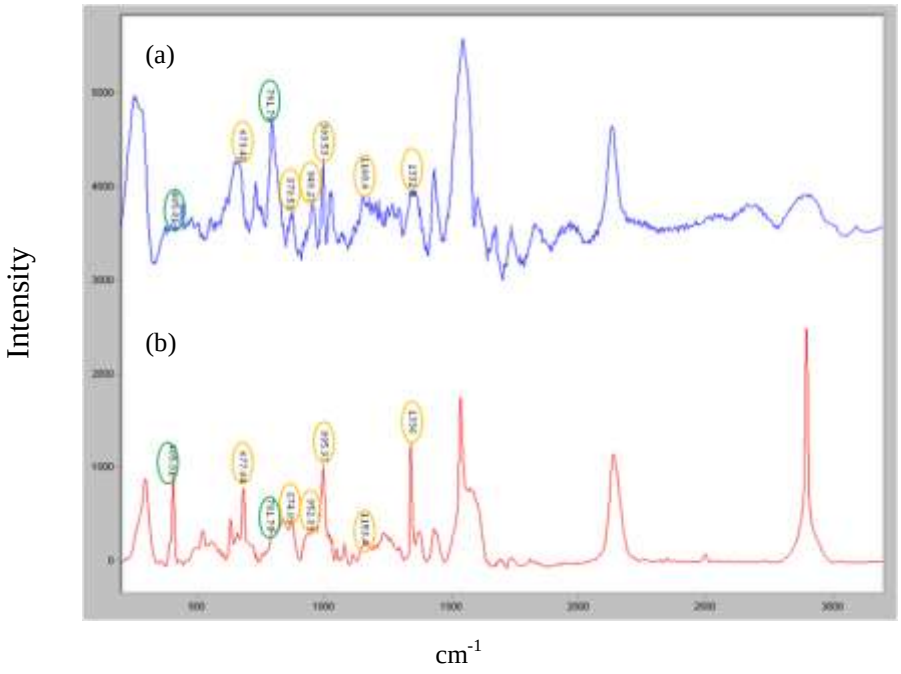

Figure 13. Identical peaks observed at 405 cm^{-1} and 791 cm^{-1} between (a) a Lorsban 75 WG sample composed of 75% chlorpyrifos and (b) a 1 µM chlorpyrifos solution. Similar peaks within 5 cm between the two samples are illustrated by yellow circles.

Table 2. Percentages of similar peaks (wave numbers) between the commercial formulations and their active ingredients. A proportional trend is observed between the percentage of similar peaks between each commercial formulation and its active ingredient versus the standard composition of each commercial formulation.

Commercial Formulation (CF)	*Active Ingredient (AI)*	*%AI (wt/wt) basis*	*% of CF SERS peaks similar to AI*
Actara 25WG	Thiamethoxam	25.0	19.35
Assail 30SG	Acetamiprid	30.0	21.43
Calypso 4F	Thiacloprid	40.4	46.67
Imidan 70W	Phosmet	70.0	73.91
Lorsban 75WG	Chlorpyrifos	75.0	40.00

Table 3. Chemical structure of each active ingredient.

Active Ingredient	Chemical Structure
Thiamethoxam	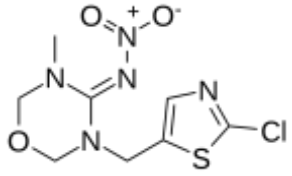
Acetamiprid	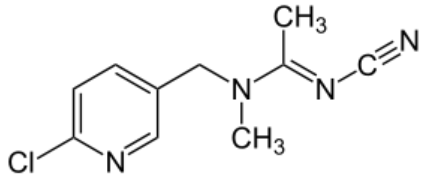
Chlorpyrifos	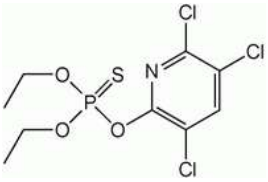
Phosmet	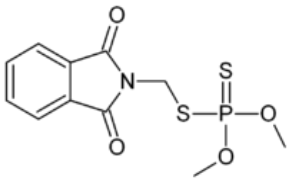
Thiacloprid	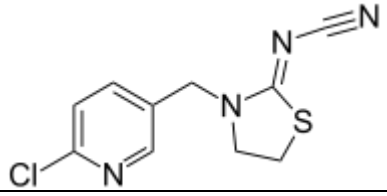

Table 4. Characteristic peaks observed for each active ingredient. Factors considered in assigning characteristic peaks included the intensity of the peak, commonality of the peak in other insecticides, and chemical structure of each active ingredient.

Active Ingredient	Characteristic Peak wave number (cm^{-1})
Thiamethoxam	**1074**
Acetamiprid	**1103**
Chlorpyrifos	**405**
Phosmet	**1776**
Thiacloprid	**684**

Table 5. Band assignments of major peaks in SERS spectra observed from each active ingredient.

Band (cm^{-1})	*Assignment*
Thiamethoxam	
469	CC torsion
677	CN bending, CC deformation
830	CC deformation
1013	CH bending
1074	CH bending
1142	CH bending, CH breathing
1289	CH bending, CN stretching
Acetamiprid	
444	CC torsion
723	CN wagging, CH wagging
917	CH wagging
927	CH wagging
1103	CH in-plane deformation, CCC in-plane deformation
1181	CH bending
1250	CN stretching
1486	CC stretching
1572	CC stretching
Chlorpyrifos	
405	Ring torsion
795	Ring deformation
1078	CH bending
1149	CH bending, CH breathing

Continued…	
Phosmet	
601	C=O in-plane deformation, vibration
666	P=S stretching
709	Benzene ring breathing
1006	Asymmetric P-O-C deformation vibration
1182	CH in P-O-CH_3 out-of-plane deformation
1250	CN in S-CH_2-N stretching
1400	CH in S-CH_2-N out-of-plane deformation
1773	C=O stretching
Thiacloprid	
684	CN bending, CC deformation
927	CH wagging
1017	CH bending
1264	CN stretching

Figures 14 to18 illustrate the successful creation of calibration curves for each active ingredient. Each calibration curve has an acceptable correlation value which represents a proper linear regression. The equations generated with each calibration curve can be utilized for quick insecticide residue analysis with a concentration as low as 250 nM (0.00025 ppm).

Apple analysis

The rinsate of each apple was analyzed using the SER-DM^{TM}. The peaks of the resulting spectra were compared with the characteristic peaks of each active ingredient. Each rinsate sample showed peaks matching the characteristic peaks of chlorpyrifos and thiacloprid. Once identical characteristic peaks were identified, the total percentage of identical peaks between the rinsate sample and the active ingredient of interest was calculated. 38.9% of chlorpyrifos' peaks were similar to the wave numbers in the spectra of the apple rinsates. 61.5% of thiacloprid's peaks were similar to the apple rinsates' spectra. Further, the linear equation from each active ingredient of interest was used to quantify the amount of insecticide residue in the rinsate sample (average). Chlorpyrifos and thiacloprid were observed in the apple rinsates at 1.1ppb and 12.4 ppb, respectively. Thus, the calibration curves were efficiently utilized in the analysis of apple samples to quantify the amount of active ingredient residue detected. The proposed method successfully permitted the detection of the residues below tolerance levels set by the EPA. The EPA tolerance levels for chlorpyrifos and thiacloprid are 10 ppb and 600 ppb, respectively. However, to confirm that the peaks analyzed in the rinsates were correctly attributed to the active ingredients and consequently that the proposed methodology can be potentially applied for the detection and quantification of samples of insecticides in fruits, further identification would be desired. In this sense, the confirmation may be performed by a complementary technique such as

mass spectrometry. Confirmation of the insecticides used by the apple supplier would also narrow the possible sources of the observed peaks.

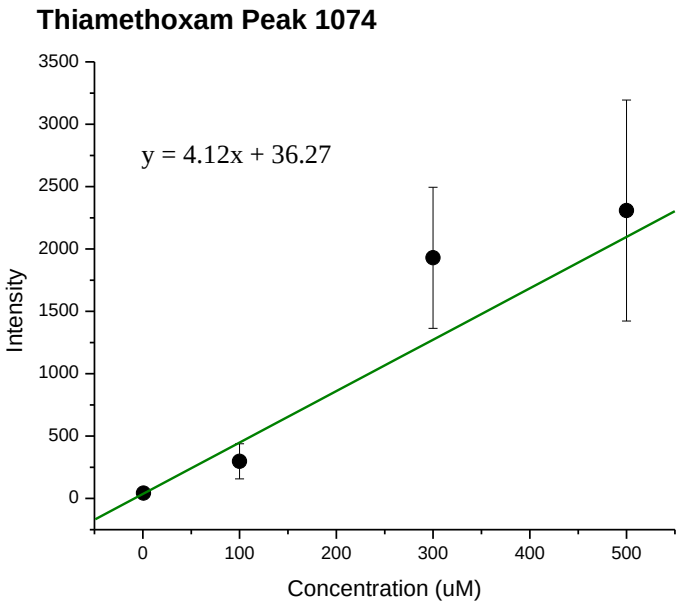

Figure 14. Calibration curve of thiamethoxam created by plotting thiamethoxam solutions at 500µM, 300µM, 100µM, and 750nM versus their respective intensities at peak 1074cm^{-1}. A linear regression value of 0.935 was observed.

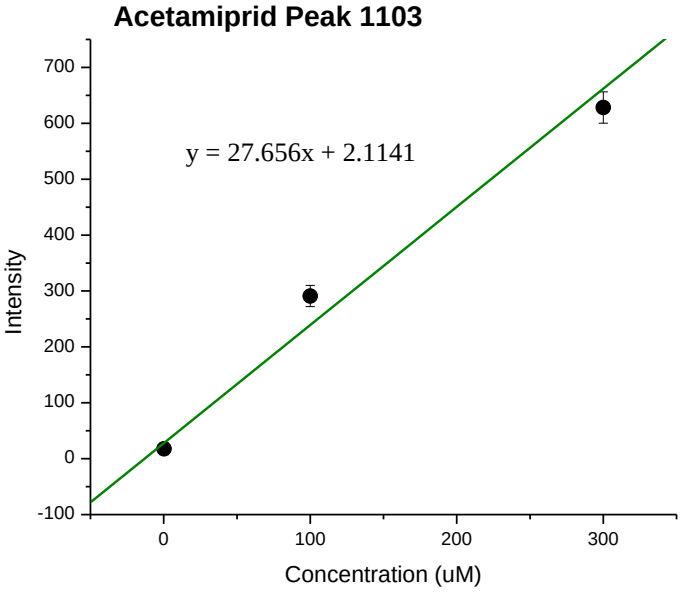

Figure 15. Calibration curve of acetamiprid developed by plotting acetamiprid solutions at 300µM, 100µM, and 250nM versus their respective intensities at peak 1103cm^{-1}. A linear regression value of 0.989 was observed.

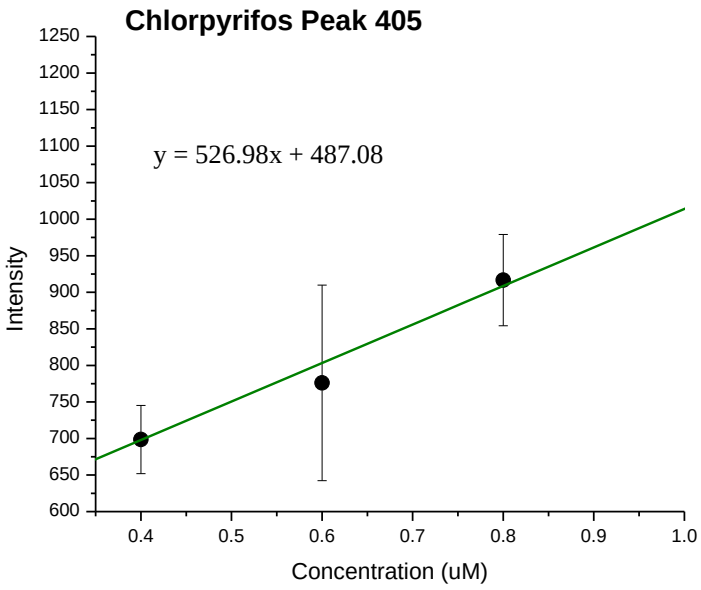

Figure 16. Calibration curve of chlorpyrifos created by plotting chlorpyrifos solutions at 800nM, 600nM, and 400nM versus their respective intensities at peak 405cm^{-1}. A linear regression value of 0.994 was observed.

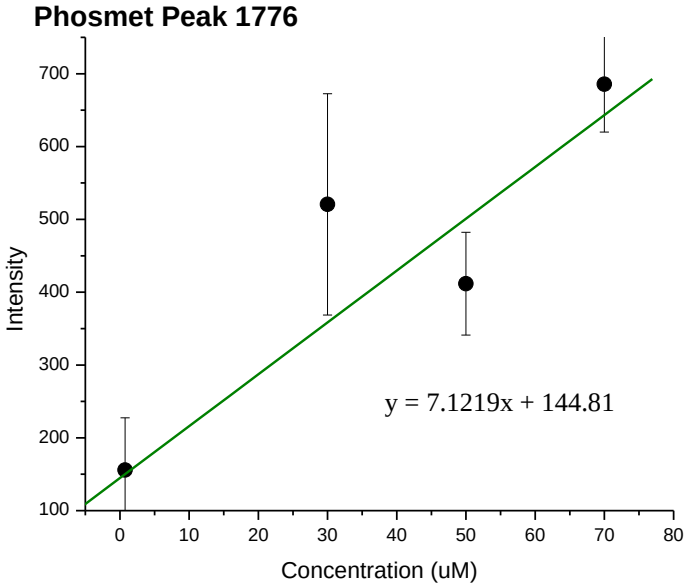

Figure 17. Calibration curve of phosmet developed by plotting phosmet solutions at 70µM, 50µM, 30µM, and 750nM versus their respective intensities at peak 1776cm^{-1}. A linear regression of 0.946 was observed.

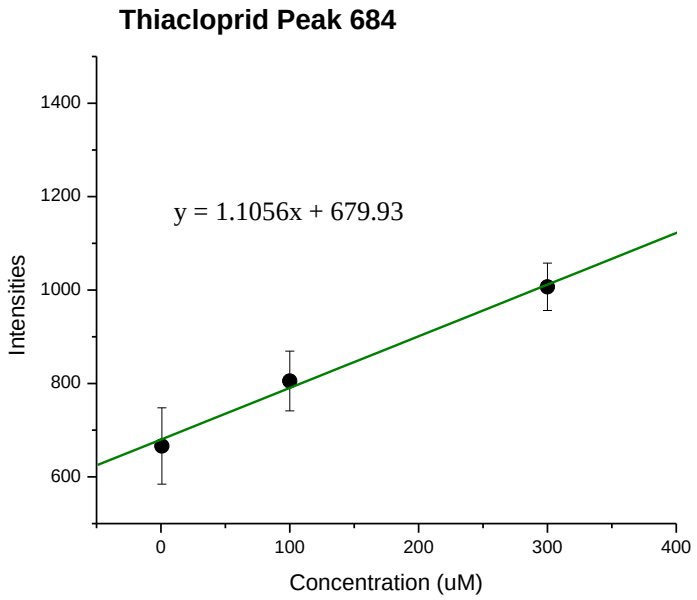

Figure 18. Calibration curve of thiacloprid created by plotting thiacloprid solutions at 300µM, 100µM, and 750nM versus their respective intensities at peak 684cm^{-1}. A linear regression value of 0.993 was observed.

CONCLUSIONS

This study presents the use of current nanotechnology in the form of SER-DM^{TM} to create calibration curves for trace insecticide detection. To illustrate the efficiency of the technology to detect the insecticides within a complex matrix, SERS spectra of commercial formulations and their respective active ingredients were analyzed. Once the active ingredients were shown to be detectable within this complex matrix, SERS spectra were obtained of each active ingredient at various concentrations. Upon completion of the spectra analysis, efficient calibration curves were generated with efficient correlation values. These curves and their respective linear equations were then shown to be efficient in quantifying possible insecticide residues on apple samples. As the need for simple, real-time analysis of trace analytes continues to flourish, techniques such as those presented in this study will be useful in fulfilling those necessities.

ACKNOWLEDGEMENTS

The author would like to thank Dr. Aaron Strickland, Dr. Cameron Bardliving, and Mike Canfield for assistance with data acquisition and analysis. The author would also like to thank David B. Combs, staff in the entomology department from the College of Agriculture and Life Sciences at Cornell University's Geneva campus, for assistance with obtaining various commercial formulations of insecticides. The author acknowledges financial support received from the United States Department of Agriculture (Grant 2009-35603-05066).

REFERENCES

1. Reichert Technologies, I., User Guide. *SR7000DC System Manual* **2012**, (2), 1-49.
2. Bantz, K. C.; Meyer, A. F.; Wittenberg, N. J.; Im, H.; Kurtulus, O.; Lee, S. H.; Lindquist, N. C.; Oh, S. H.; Haynes, C. L., Recent progress in SERS biosensing. *Physical Chemistry Chemical Physics* **2011,** 13, (24), 11551-11567.
3. Ding, X. K.; Zhang, W.; Cheng, D.; He, J. Z.; Yang, K. L., Oligopeptides functionalized surface plasmon resonance biosensors for detecting thiacloprid and imidacloprid. *Biosensors & Bioelectronics* **2012,** 35, (1), 271-276.
4. Fu, G. L.; Chen, W. W.; Yue, X. L.; Jiang, X. Y., Highly sensitive colorimetric detection of organophosphate pesticides using copper catalyzed click chemistry. *Talanta* **2013,** 103, 110-115.
5. Shamsipur, M.; Sarkouhi, M.; Hassan, J., Selective Monitoring of Organophosphorus Pesticides by P-31-NMR Spectroscopy: Application to Purity Assay of Technical Products and Concentration Determination of Formulated Samples. *Applied Magnetic Resonance* 42, (2), 227-237.
6. Yang, J.; Wang, H.; Xu, W.; Hao, D.; Du, L.; Zhao, X.; Sun, C., Metabolomic analysis of rat plasma following chronic low-dose exposure to dichlorvos. *Human & Experimental Toxicology* **2012,** 32, (2), 196-205.
7. Stiles, P. L.; Dieringer, J. A.; Shah, N. C.; Van Duyne, R. R., Surface-Enhanced Raman Spectroscopy. In *Annual Review of Analytical Chemistry*, 2008; Vol. 1, pp 601-626.
8. Raman, C. V.; Krishnan, K. S., A new type of secondary radiation. *Nature* **1928,** 121, 501-502.
9. Raman, C. V., The Raman effect. Investigation of molecular structure by light scattering. *Transactions of the Faraday Society* **1929,** 25, 0781-0791.
10. Raman, C. V.; Krishnan, K. S., The optical analogue of the Compton effect. *Nature* **1928,** 121, 711-711.
11. Landsberg, G.; Mandelstam, L., A novel effect of light scattering in crystals. *Naturwissenschaften* **1928**, (16), 557.
12. Albrecht, M. G.; Creighton, J. A., Anomalously Intense Raman-Spectra of Pyridine at a Silver Electrode. *Journal of the American Chemical Society* **1977,** 99, (15), 5215-5217.
13. Fleischm.M; Hendra, P. J.; McQuilla.Aj, Raman-Spectra of Pyridine Adsorbed at a Silver Electrode. *Chemical Physics Letters* **1974,** 26, (2), 163-166.
14. Jeanmaire, D. L.; Van Duyne, R. P., Surface raman spectroelectrochemistry:Part I. Heterocyclic, aromatic, and aliphatic amines adsorbed on the anodized silver electrode. *JEC Journal of Electroanalytical Chemistry* **1977,** 84, (1), 1-20.
15. Wu, D. Y.; Li, J. F.; Ren, B.; Tian, Z. Q., Electrochemical surface-enhanced Raman spectroscopy of nanostructures. *Chemical Society Reviews* **2008,** 37, (5), 1025-1041.
16. Campion, A.; Kambhampati, P., Surface-enhanced Raman scattering. *Chemical Society Reviews* **1998,** 27, (4), 241-250.
17. Bompart, M.; De Wilde, Y.; Haupt, K., Chemical Nanosensors Based on Composite Molecularly Imprinted Polymer Particles and Surface-Enhanced Raman Scattering. *Advanced Materials* **2010,** 22, (21), 2343-2348.
18. Banholzer, M. J.; Millstone, J. E.; Qin, L. D.; Mirkin, C. A., Rationally designed nanostructures for surface-enhanced Raman spectroscopy. *Chemical Society Reviews* **2008,** 37, (5), 885-897.

19. Cialla, D.; Marz, A.; Bohme, R.; Theil, F.; Weber, K.; Schmitt, M.; Popp, J., Surface-enhanced Raman spectroscopy (SERS): progress and trends. *Analytical and Bioanalytical Chemistry* **2012,** 403, (1), 27-54.
20. Freeman, R. G.; Grabar, K. C.; Allison, K. J.; Bright, R. M.; Davis, J. A.; Guthrie, A. P.; Hommer, M. B.; Jackson, M. A.; Smith, P. C.; Walter, D. G.; Natan, M. J., Self-Assembled Metal Colloid Monolayers - An Approach to SERS Substrates. *Science* **1995,** 267, (5204), 1629-1632.
21. Maxwell, D. J.; Emory, Sr.; Nie, S. M., Nanostructured thin-film materials with surface-enhanced optical properties. *Chemistry of Materials* **2001,** 13, (3), 1082-1088.
22. Dick, L. A.; McFarland, A. D.; Haynes, C. L.; Van Duyne, R. P., Metal Film over Nanosphere (MFON) Electrodes for Surface-Enhanced Raman Spectroscopy (SERS): Improvements in Surface Nanostructure Stability and Suppression of Irreversible Loss. *J. Phys. Chem. B The Journal of Physical Chemistry B* **2002,** 106, (4), 853-860.
23. Gunnarsson, L.; Bjerneld, E. J.; Xu, H.; Petronis, S.; Kasemo, B.; Kall, M., Interparticle coupling effects in nanofabricated substrates for surface-enhanced Raman scattering. *Applied Physics Letters* **2001,** 78, (6), 802-804.
24. Jackson, J. B.; Halas, N. J., Surface-enhanced Raman scattering on tunable plasmonic nanoparticle substrates. *Proceedings of the National Academy of Sciences of the United States of America* **2004,** 101, (52), 17930-17935.
25. Tripp, R. A.; Dluhy, R. A.; Zhao, Y. P., Novel nanostructures for SERS biosensing. *Nano Today* **2008,** 3, (3-4), 31-37.
26. Chen, L. M.; Liu, Y. N., Surface-Enhanced Raman Detection of Melamine on Silver-Nanoparticle-Decorated Silver/Carbon Nanospheres: Effect of Metal Ions. *Acs Applied Materials & Interfaces* **2011,** 3, (8), 3091-3096.
27. Lee, J. H.; Nam, J. M.; Jeon, K. S.; Lim, D. K.; Kim, H.; Kwon, S.; Lee, H.; Suh, Y. D., Tuning and Maximizing the Single-Molecule Surface-Enhanced Raman Scattering from DNA-Tethered Nanodumbbells. *Acs Nano* **2012,** 6, (11), 9574-9584.
28. Zhang, K.; Xiang, Y. J.; Wu, X. C.; Feng, L. L.; He, W. W.; Liu, J. B.; Zhou, W. Y.; Xie, S. S., Enhanced Optical Responses of Au@Pd Core/Shell Nanobars. *Langmuir* **2009,** 25, (2), 1162-1168.
29. Aggarwal, R. L.; Farrar, L. W.; Greeneltch, N. G.; Van Duyne, R. P.; Polla, D. L., Measurement of the Surface-Enhanced Coherent Anti-Stokes Raman Scattering (SECARS) Due to the 1574 cm(-1) Surface-Enhanced Raman Scattering (SERS) Mode of Benzenethiol Using Low-Power (< 20 mW) CW Diode Lasers. *Applied Spectroscopy* **2013,** 67, (2), 132-135.
30. Hao, J. M.; Han, M. J.; Li, J. W.; Meng, X. G., Surface modification of silver nanofilms for improved perchlorate detection by surface-enhanced Raman scattering. *Journal of Colloid and Interface Science* **2012,** 377, 51-57.
31. Kahraman, M.; Cakmakyapan, S.; Ozbay, E.; Culha, M., An array of surface-enhanced Raman scattering substrates based on plasmonic lenses. *Annalen Der Physik* **2012,** 524, (11), 663-669.
32. Voiciuk, V.; Valincius, G.; Budvytyte, R.; Matijoska, A.; Matulaitiene, I.; Niaura, G., Surface-enhanced Raman spectroscopy for detection of toxic amyloid beta oligomers adsorbed on self-assembled monolayers. *Spectrochimica Acta Part a-Molecular and Biomolecular Spectroscopy* **2012,** 95, 526-532.

33. Wang, Y. L.; Salehi, M.; Schutz, M.; Rudi, K.; Schlucker, S., Microspectroscopic SERS detection of interleukin-6 with rationally designed gold/silver nanoshells. *Analyst* **2013,** 138, (6), 1764-1771.
34. Vongsvivut, J.; Robertson, E. G.; McNaughton, D., Surface-enhanced Raman spectroscopic analysis of fonofos pesticide adsorbed on silver and gold nanoparticles. *Journal of Raman Spectroscopy* **2009,** 41, (10), 1137-1148.
35. Mosier-Boss, P. A., Optical properties of surface-enhanced Raman-active capture matrices. *Applied Spectroscopy* **2006,** 60, (10), 1148-1156.
36. DeVault, G. L.; Sepaniak, M. J., Spatially focused deposition of capillary electrophoresis effluent onto surface-enhanced Raman-active substrates for off-column spectroscopy. *Electrophoresis* **2001,** 22, (11), 2303-2311.
37. Stokes, D. L.; Alarie, J. P.; Ananthanarayanan, V.; Vo-Dinh, T., Fiber optic SERS sensor for environmental monitoring [3534-86]. *Proceedings- SPIE the International Society for Optical Engineering* **1999**, (3534), 647-654.
38. Kundu, S.; Mandal, M.; Ghosh, S. K.; Pal, T., Photochemical deposition of SERS active silver nanoparticles on silica gel. *Journal of Photochemistry and Photobiology A* **2004,** 162, (2-3), 625-632.
39. Strickland, A. D.; Batt, C. A., Detection of Carbendazim by Surface-Enhanced Raman Scattering Using Cyclodextrin Inclusion Complexes on Gold Nanorods. *Analytical Chemistry* **2009,** 81, (8), 2895-2903.
40. Barahona, Aptasensor based on polymer-gold nanoparticles composite microspheres for the detection of malathion using surface enhanced raman spectroscopy. *Industrial Biotechnology* **2013,** 9, (1), 42-50.
41. Mecker, L. C.; Tyner, K. M.; Kauffman, J. F.; Arzhantsev, S.; Mans, D. J.; Gryniewicz-Ruzicka, C. M., Selective melamine detection in multiple sample matrices with a portable Raman instrument using surface enhanced Raman spectroscopy-active gold nanoparticles. *Analytica Chimica Acta* **2012,** 733, 48-55.
42. iFyber, L. Surface enhanced diagnostic membranes (February 19),
43. Ryu, K.; Haes, A. J.; Park, H. Y.; Nah, S.; Kim, J.; Chung, H.; Yoon, M. Y.; Han, S. H., Use of peptide for selective and sensitive detection of an Anthrax biomarker via peptide recognition and surface-enhanced Raman scattering. *Journal of Raman Spectroscopy* **2010,** 41, (2), 121-124.
44. Zheng, R.; Park, B. W.; Kim, D. S.; Cameron, B. D., Development of a highly specific amine-terminated aptamer functionalized surface plasmon resonance biosensor for blood protein detection. *Biomedical Optics Express* **2011,** 2, (9), 2731-2740.
45. Narsaiah, K.; Jha, S. N.; Bhardwaj, R.; Sharma, R.; Kumar, R., Optical biosensors for food quality and safety assurance-a review. *Journal of Food Science and Technology-Mysore* **2012,** 49, (4), 383-406.
46. Lahiri, J.; Isaacs, L.; Tien, J.; Whitesides, G. M., A strategy for the generation of surfaces presenting ligands for studies of binding based on an active ester as a common reactive intermediate: A surface plasmon resonance study. *Analytical Chemistry* **1999,** 71, (4), 777-790.
47. Liedberg, B.; Nylander, C.; Lundstrom, I., Surface-Plasmon Resonance for Gas-Detection and Biosensing. *Sensors and Actuators* **1983,** 4, (2), 299-304.
48. Flatmark, T.; Stokka, A. J.; Berge, S. V., Use of surface plasmon resonance for real-time measurements of the global conformational transition in human phenylalanine hydroxylase in

response to substrate binding and catalytic activation. *Analytical Biochemistry* **2001,** 294, (2), 95-101.
49. Gershon, P. D.; Khilko, S., Stable Chelating Linkage for Reversible Immobilization of Oligohistidine Tagged Proteins in the Biacore Surface-Plasmon Resonance Detector. *Journal of Immunological Methods* **1995,** 183, (1), 65-76.
50. Yang, G.; Kang, S., SPR-based antibody-antigen interaction for real time analysis of carbamate pesticide residues. *Food Science and Biotechnology* **2008,** 17, (1), 15-19.
51. Bora, M.; Celebi, K.; Zuniga, J.; Watson, C.; Milaninia, K. M.; Baldo, M. A., Near field detector for integrated surface plasmon resonance biosensor applications. *Optics Express* **2009,** 17, (1), 329-336.
52. Mauriz, E.; Calle, A.; Lechuga, L. M.; Quintana, J.; Montoya, A.; Manclus, J. J., Real-time detection of chlorpyrifos at part per trillion levels in ground, surface and drinking water samples by a portable surface plasmon resonance immunosensor. *Analytica Chimica Acta* **2006,** 561, (1-2), 40-47.
53. Meneely, J. P.; Ricci, F.; Vesco, S.; Abouzied, M.; Sulyok, M.; Krska, R.; Elliott, C. T., A comparative study of qualitative immunochemical screening assays for the combined measurement of T-2/HT-2 in cereals and cereal-based products. *World Mycotoxin Journal* **2011,** 4, (4), 385-394.
54. Naimushin, A. N.; Soelberg, S. D.; Bartholomew, D. U.; Elkind, J. L.; Furlong, C. E., A portable surface plasmon resonance (SPR) sensor system with temperature regulation. *Sensors and Actuators B-Chemical* **2003,** 96, (1-2), 253-260.
55. Sohn, Y.-S., A Portable Surface Plasmon Resonance Sensor for a Diagnostic Tool. *Sensor Letters* **2011,** 9, (1), 272-275.
56. Lin, H.-Y.; Tsao, Y.-C.; Tsai, W.-H.; Yang, Y.-W.; Yan, T.-R.; Sheu, B.-C., Development and application of side-polished fiber immunosensor based on surface plasmon resonance for the detection of Legionella pneumophila with halogens light and 850 nm-LED. *Sensors and Actuators a-Physical* **2007,** 138, (2), 299-305.
57. Yu-Cheng, L.; Yu-Chia, T.; Woo-Hu, T.; Tsui-Shan, H.; Ko-Shao, C.; Shu-Chuan, L., The enhancement method of optical fiber biosensor based on surface plasmon resonance with cold plasma modification. *Sensors and Actuators B-Chemical* **2008,** 133, (2), 370-373.
58. Xiao, C.; Jiang, F.; Zhou, B.; Li, R.; Liu, Y., Immobilization of Escherichia coli for detection of phage T4 using surface plasmon resonance. *Science China-Chemistry* **2012,** 55, (9), 1931-1939.
59. Henseleit, A.; Schmieder, S.; Bley, T.; Sonntag, F.; Schilling, N.; Quenzel, P.; Danz, N.; Klotzbach, U.; Boschke, E., A compact and rapid aptasensor platform based on surface plasmon resonance. *Engineering in Life Sciences* **2011,** 11, (6), 573-579.
60. Kim, Y. R.; Paik, H. J.; Ober, C. K.; Coates, G. W.; Mark, S. S.; Ryan, T. E.; Batt, C. A., Real-time analysis of enzymatic surface-initiated polymerization using surface plasmon resonance (SPR). *Macromolecular Bioscience* **2006,** 6, (2), 145-152.
61. Mani, R. J.; Dye, R. G.; Snider, T. A.; Wang, S.; Clinkenbeard, K. D., Bi-cell surface plasmon resonance detection of aptamer mediated thrombin capture in serum. *Biosensors & Bioelectronics* **2011,** 26, (12), 4832-4836.
62. Jalit, Y.; Gutierrez, F. A.; Dubacheva, G.; Goyer, C.; Coche-Guerente, L.; Defrancq, E.; Labbe, P.; Rivas, G. A.; Rodriguez, M. C., Characterization of a modified gold platform for the development of a label-free anti-thrombin aptasensor. *Biosensors & Bioelectronics* **2013,** 41, 424-429.

63. Tran, D. T.; Knez, K.; Janssen, K. P.; Pollet, J.; Spasic, D.; Lammertyn, J., Selection of aptamers against Ara h 1 protein for FO-SPR biosensing of peanut allergens in food matrices. *Biosensors & Bioelectronics* **2012,** 43, 245-51.
64. Wang, Y.; Ye, Z.; Si, C.; Ying, Y., Monitoring of Escherichia coli O157:H7 in food samples using lectin based surface plasmon resonance biosensor. *Food Chemistry* **2013,** 136, (3-4), 1303-1308.
65. Daniel, C.; Melaine, F.; Roupioz, Y.; Livache, T.; Buhot, A., Real time monitoring of thrombin interactions with its aptamers: Insights into the sandwich complex formation. *Biosensors & Bioelectronics* **2013,** 40, (1), 186-192.
66. Park, B. J.; Sa, Y. S.; Kim, Y. H.; Kim, Y., Spectroscopic and Electrochemical Detection of Thrombin/5 '-SH or 3 '-SH Aptamer Immobilized on (porous) Gold Substrates. *Bulletin of the Korean Chemical Society* **2012,** 33, (1), 100-104.
67. Ruark, C. D.; Hack, C. E.; Robinson, P. J.; Anderson, P. E.; Gearhart, J. M., Quantitative structure-activity relationships for organophosphates binding to acetylcholinesterase. *Archives of Toxicology* **2013,** 87, (2), 281-289.
68. Fukuto, T. R., Mechanism of Action of Organophosphorus and Carbamate Insecticides. *Environmental Health Perspectives* **1990,** 87, 245-254.
69. Grigoryan, H.; Schopfer, L. M.; Peeples, E. S.; Duysen, E. G.; Grigoryan, M.; Thompson, C. M.; Lockridge, O., Mass spectrometry identifies multiple organophosphorylated sites on tubulin. *Toxicology and Applied Pharmacology* **2009,** 240, (2), 149-158.
70. Gallo, M. A.; Lawryk, N. J., Organic phosphorus pesticides. *Handbook of pesticide toxicology: classes of pesticides* **1991,** 2, 917-1123.
71. Tucker, J. B., *War of nerves : chemical warfare from World War I to al-Qaeda*. Pantheon Books: New York, 2006.
72. Cooper, J.; Dobson, H., The benefits of pesticides to mankind and the environment. *Crop Protection* **2007,** 26, (9), 1337-1348.
73. Chakraborty, S.; Mukherjee, S.; Roychoudhury, S.; Siddique, S.; Lahiri, T.; Ray, M. R., Chronic Exposures to Cholinesterase-inhibiting Pesticides Adversely Affect Respiratory Health of Agricultural Workers in India. *Journal of Occupational Health* **2009,** 51, (6), 488-497.
74. Hancock, D. B.; Martin, E. R.; Mayhew, G. M.; Stajich, J. M.; Jewett, R.; Stacy, M. A.; Scott, B. L.; Vance, J. M.; Scott, W. K., Pesticide exposure and risk of Parkinson's disease: A family-based case-control study. *Bmc Neurology* **2008,** 8, 12.
75. Hayden, K. M.; Welsh-Bohmer, K. A.; Darcey, D.; Ostbye, T.; Norton, M. C.; Zandi, P. P.; Breitner, J. C. S., Occupational exposure to pesticides increases the risk of incident AD: The Cache County Study. *Neurology Neurology* **2010,** 74, (19), 1524-1530.
76. Slotkin, T. A., Does early-life exposure to organophosphate insecticides lead to prediabetes and obesity? *Reproductive Toxicology* **2011,** 31, (3), 297-301.
77. Okamura, A.; Saito, I.; Ueyama, J.; Ito, Y.; Nakajima, T.; Kamijima, M., New analytical method for sensitive quantification of urinary 3-methyl-4-nitrophenol to assess fenitrothion exposure in general population and occupational sprayers. *Toxicology Letters* **2012,** 210, (2), 220-224.
78. Fuentes-Matus, C.; Vega y Leon, S.; Diaz-Gonzalez, G.; Noa-Perez, M.; Gutierrez-Tolentino, R., Determination of Residues of Malathion and Malaoxon in Mango Varieties Ataulfo and Tommy Atkins Produced in Chahuites, Oaxaca. *Agrociencia* **2010,** 44, (2), 215-223.

79. Sinha, S. N.; Rao, M. V. V.; Vasudev, K.; Odetokun, M., A liquid chromatography mass spectrometry-based method to measure organophosphorous insecticide, herbicide and non-organophosphorous pesticide in grape and apple samples. *Food Control* **2012,** 25, (2), 636-646.
80. Tomizawa, M.; Casida, J. E., Neonicotinoid insecticide toxicology: Mechanisms of selective action. In *Annual Review of Pharmacology and Toxicology*, 2005; Vol. 45, pp 247-+.
81. Soloway, S. B.; Henry, A. C.; W.D., K., Nitromethylene insecticides. *Advances in Pesticide Science* **1979,** 2, 206-217.
82. Kollmeyer, W. D.; Flattum, R. F.; Foster, J. P., Discovery of nitromethylene heterocycle insecticides. *Nicotinoid Insecticides and the Nicotinic Acetylcholine Receptor* **1999**, 71-89.
83. Cutler, P.; Slater, R.; Edmunds, A. J. F.; Maienfisch, P.; Hall, R. G.; Earley, F. G. P.; Pitterna, T.; Pal, S.; Paul, V.-L.; Goodchild, J.; Blacker, M.; Hagmann, L.; Crossthwaite, A. J., Investigating the mode of action of sulfoxaflor: a fourth-generation neonicotinoid. *Pest. Manag. Sci Pest Management Science* **2012**, (2), n/a.
84. Xu, T.; Xu, Q. G.; Li, H.; Wang, J.; Li, Q. X.; Shelver, W. L.; Li, J., Strip-based immunoassay for the simultaneous detection of the neonicotinoid insecticides imidacloprid and thiamethoxam in agricultural products. *Talanta* **2012,** 101, 85-90.
85. Watanabe, E.; Kobara, Y.; Miyake, S., Validation of a commercial ELISA for the analysis of the insecticide dinotefuran in a variety of analytically challenging vegetables. *Food Additives and Contaminants Part a-Chemistry Analysis Control Exposure & Risk Assessment* **2012,** 29, (7), 1067-1073.
86. Seccia, S.; Fidente, P.; Montesano, D.; Morrica, P., Determination of neonicotinoid insecticides residues in bovine milk samples by solid-phase extraction clean-up and liquid chromatography with diode-array detection. *Journal of Chromatography A* **2008,** 1214, (1-2), 115-120.
87. Aragay, G.; Pino, F.; Merkoci, A., Nanomaterials for Sensing and Destroying Pesticides. *Chemical Reviews* **2012,** 112, (10), 5317-5338.
88. Boro, R. C.; Kaushal, J.; Nangia, Y.; Wangoo, N.; Bhasin, A.; Suri, C. R., Gold nanoparticles catalyzed chemiluminescence immunoassay for detection of herbicide 2,4-dichlorophenoxyacetic acid. *Analyst* **2011,** 136, (10), 2125-2130.
89. Fodjo, E. K.; Riaz, S.; Li, D. W.; Qu, L. L.; Marius, N. P.; Albert, T.; Long, Y. T., Cu@Ag/beta-AgVO3 as a SERS substrate for the trace level detection of carbamate pesticides. *Analytical Methods* **2012,** 4, (11), 3785-3791.
90. Kim, S. J.; Gobi, K. V.; Tanaka, H.; Shoyama, Y.; Miura, N., A simple and versatile self-assembled monolayer based surface plasmon resonance immunosensor for highly sensitive detection of 2,4-D from natural water resources. *Sensors and Actuators B-Chemical* **2008,** 130, (1), 281-289.
91. Ferrer, I.; Thurman, E. M.; Fernandez-Alba, A. R., Quantitation and accurate mass analysis of pesticides in vegetables by LC/TOF-MS. *Analytical Chemistry* **2005,** 77, (9), 2818-2825.
92. Lee, J. K.; Ahn, K. C.; Park, O. S.; Kang, S. Y.; Hammock, B. D., Development of an ELISA for the detection of the residues of the insecticide imidacloprid in agricultural and environmental samples. *Journal of Agricultural and Food Chemistry* **2001,** 49, (5), 2159-2167.
93. Navalon, A.; GonzalezCasado, A.; ElKhattabi, R.; Vilchez, J. L.; FernandezAlba, A. R., Determination of imidacloprid in vegetable samples by gas chromatography-mass spectrometry. *Analyst* **1997,** 122, (6), 579-581.

94. Obana, H.; Okihashi, M.; Akutsu, K.; Kitagawa, Y.; Hori, S., Determination of neonicotinoid pesticide residues in vegetables and fruits with solid phase extraction and liquid chromatography mass spectrometry. *Journal of Agricultural and Food Chemistry* **2003,** 51, (9), 2501-2505.
95. Pang, G. F.; Liu, Y. M.; Fan, C. L.; Zhang, J. J.; Cao, Y. Z.; Li, X. M.; Li, Z. Y.; Wu, Y. P.; Guo, T. T., Simultaneous determination of 405 pesticide residues in grain by accelerated solvent extraction then gas chromatography-mass spectrometry or liquid chromatography-tandem mass spectrometry. *Analytical and Bioanalytical Chemistry* **2006,** 384, (6), 1366-1408.
96. Bruno, J. G.; Carrillo, M. P.; Phillips, T.; King, B., Development of DNA aptamers for cytochemical detection of acetylcholine. *In Vitro Cellular & Developmental Biology-Animal* **2008,** 44, (3-4), 63-72.
97. Balamurugan, S.; Obubuafo, A.; Soper, S. A.; McCarley, R. L.; Spivak, D. A., Designing highly specific biosensing surfaces using aptamer monolayers on gold. *Langmuir* **2006,** 22, (14), 6446-6453.
98. Bardin, P. G.; Vaneeden, S. F.; Moolman, J. A.; Foden, A. P.; Joubert, J. R., Organophosphate and Carbamate Poisoning. *Archives of Internal Medicine* **1994,** 154, (13), 1433-1441.
99. Collombet, J. M., Nerve agent intoxication: Recent neuropathophysiological findings and subsequent impact on medical management prospects. *Toxicology and Applied Pharmacology* **2011,** 255, (3), 229-241.
100. Aroca, R. F.; Clavijo, R. E.; Halls, M. D.; Schlegel, H. B., Surface-enhanced Raman spectra of phthalimide. Interpretation of the SERS spectra of the surface complex formed on silver islands and colloids. *Journal of Physical Chemistry A* **2000,** 104, (42), 9500-9505.
101. Liu, B.; Zhou, P.; Liu, X. M.; Sun, X.; Li, H.; Lin, M. S., Detection of Pesticides in Fruits by Surface-Enhanced Raman Spectroscopy Coupled with Gold Nanostructures. *Food and Bioprocess Technology* **2013,** 6, (3), 710-718.
102. Mary, Y. S.; Raju, K.; Yildiz, I.; Temiz-Arpaci, O.; Nogueira, H. I. S.; Granadeiro, C. M.; Van Alsenoy, C., FT-IR, FT-Raman, SERS and computational study of 5-ethylsulphonyl-2-(o-chlorobenzyl)benzoxazole. *Spectrochimica Acta Part a-Molecular and Biomolecular Spectroscopy* **2012,** 96, 617-625.